Mon. Not. R. astr. Soc. (1987) **227**, 563–588

An infrared–optical study of *IRAS* point sources in the Virgo region

S. K. Leggett[1], R. G. Clowes[2], M. Kalafi[3]★, H. T. MacGillivray[2], P. J. Puxley[1], A. Savage[2]† and R. D. Wolstencroft[2]
[1]*Astronomy Department, University of Edinburgh, Blackford Hill, Edinburgh EH9 3HJ*
[2]*Royal Observatory, Blackford Hill, Edinburgh EH9 3HJ*
[3]*Department of Astronomy, Tabriz University, Iran*

Accepted 1987 March 3. Received 1987 February 10

Summary. Optical identifications are given for 199 of the 206 point sources detected by the *Infrared Astronomical Satellite* (*IRAS*) in a 113 deg^2 area centred on the Virgo cluster. The identifications are made using four deep IIIa-J plates taken with the 1.2-m UK Schmidt Telescope. Fifty-four of the sources are associated with stars, 113 with optically bright (B_J<16) galaxies, 32 with faint (B_J>16) galaxies, and seven are apparently empty fields, to the plate limit of B=22. This area is affected by infrared cirrus, with which five of the seven empty fields are associated.

We have created an infrared–optical Virgo galaxy database, complete to about B=16, by combining our data with the catalogue of Binggeli, Sandage & Tammann. The *IRAS* galaxy sources are dominated by spirals; only 4 per cent of the E and S0 galaxies brighter than B=16 are detected, compared with 44 per cent of the Sc galaxies. We find that the infrared properties of the Virgo cluster galaxies are indistinguishable from those of field galaxies at similar redshifts. Such *IRAS* galaxies are typically spirals with $B \leqslant 14$, ratios of $F(100\mu\mathrm{m})/F(60\mu\mathrm{m}) \sim 3$ and of infrared to optical luminosity of about 1, with an infrared luminosity of $\sim 10^9 L_\odot$. These properties are independent of neutral hydrogen content for the Virgo cluster galaxies. The ratios $L(\mathrm{IR})/L(B)$ and $F(100\mu\mathrm{m})/F(60\mu\mathrm{m})$ are correlated with $L(\mathrm{IR})$, implying that the optically faint field galaxies have $L(\mathrm{IR}) > 10^{12} L_\odot$.

1 Introduction

This is the second paper reporting the results of a large-scale programme underway at Edinburgh to identify optically *IRAS* point sources. The *Infrared Astronomical Satellite* is described in detail in the Explanatory Supplement edited by Beichman *et al.* 1985 (hereafter *IRAS* ES). Paper 1

★Visiting Professor at ROE.
†Present address: UK Schmidt Telescope Unit, Coonabarabran, NSW, Australia.

(Wolstencroft *et al.* 1986) give optical identifications for 312 *IRAS* point sources in a 304 deg^2 area at the South Galactic Pole (SGP).

IRAS sources at high galactic latitudes have also been studied by Lawrence *et al.* (1986), but they deliberately avoided the Virgo cluster, concentrating on field galaxies. This cluster of nearby bright galaxies can, however, be used to study the effect of environment on *IRAS* galaxies, and the wealth of published data on the cluster has enabled us to create a very useful infrared–optical database.

The identification procedure used here is semi-automatic. The central 29 deg^2 of each 41 deg^2 SERC IIIa-J Schmidt glass atlas plate are digitized by the plate measuring machine COSMOS. The COSMOS system has been recently reviewed by MacGillivray & Stobie (1984). Objects within a 1 arcmin radius of the *IRAS* point source (IRPS) position are extracted using STARLINK supported catalogue handling software, with additional programs written by one of us (RGC) specifically for this project.

The candidates are inspected by eye using plate overlays. Identifications with bright stars are unambiguous, and these give the initial positional errors for the field, which then allow identification of the other sources. This process is usually straightforward, and the *IRAS* flux distribution can be used to confirm the candidate.

This paper presents identifications for the *IRAS* point sources from four plates centred on the Virgo cluster region, which cover the sky area given by a right ascension range $12^h 02^m$ to $12^h 47^m$, and a declination range 7° 59′ to 18° 38′. This region is 113 square degrees in area and contains 206 *IRAS* point sources. The source density of 1.8 per square degree compares with 1.1 per square degree at the SGP (Paper 1). The increase in density is due to the cluster galaxies only – the stellar density is very similar as would be expected since this area is near the North Galactic Pole (galactic latitude about 80°).

The identifications are given in Section 2, where the positional errors and confidence limits are described. Properties of the empty fields are discussed in Section 3, the stellar sources in Section 4, and the galaxies in Section 5.

We have paired our data with the optical catalogue of Virgo galaxies by Binggeli, Sandage & Tammann (1985), which covers 77 per cent of the area studied in this work. This has allowed us to investigate, in Section 5, the properties of *IRAS* galaxies and non-*IRAS* galaxies, as well as cluster members and field galaxies.

The Virgo cluster region on IIIa-J plates is shown in Plate 1; this shows the area covered by this work. The region of overlap with Binggeli *et al.* is indicated on this plate. Plate 2 shows the *IRAS* skyflux image at 100 μm on which the brightest galaxies can be seen, and on which the positions of the seven empty fields (see Section 3) have been marked. This plate also shows that the region is affected by infrared cirrus, the diffuse extended structure that may appear as point sources at 60 or 100 μm. The 60 μm skyflux image shows the brighter galaxies and slight traces of cirrus; the 25 and 12 μm images show a few stellar sources. Comparison of Plates 1 and 2 shows that *IRAS* detected the optically bright spiral galaxies (see Section 5.3 for detailed discussion).

2 The identifications

The identifications are given in Table 1, which gives the following information.

Column 1: *IRAS* name, abbreviated right ascension and declination HHMM.M±DDMM.
Columns 2, 3: optical position, measured by COSMOS (1950). For empty fields the *IRAS* position is given in brackets.
Columns 4, 5: positional difference (optical–IRPS position), arcsec.
Column 6: name of optical source.

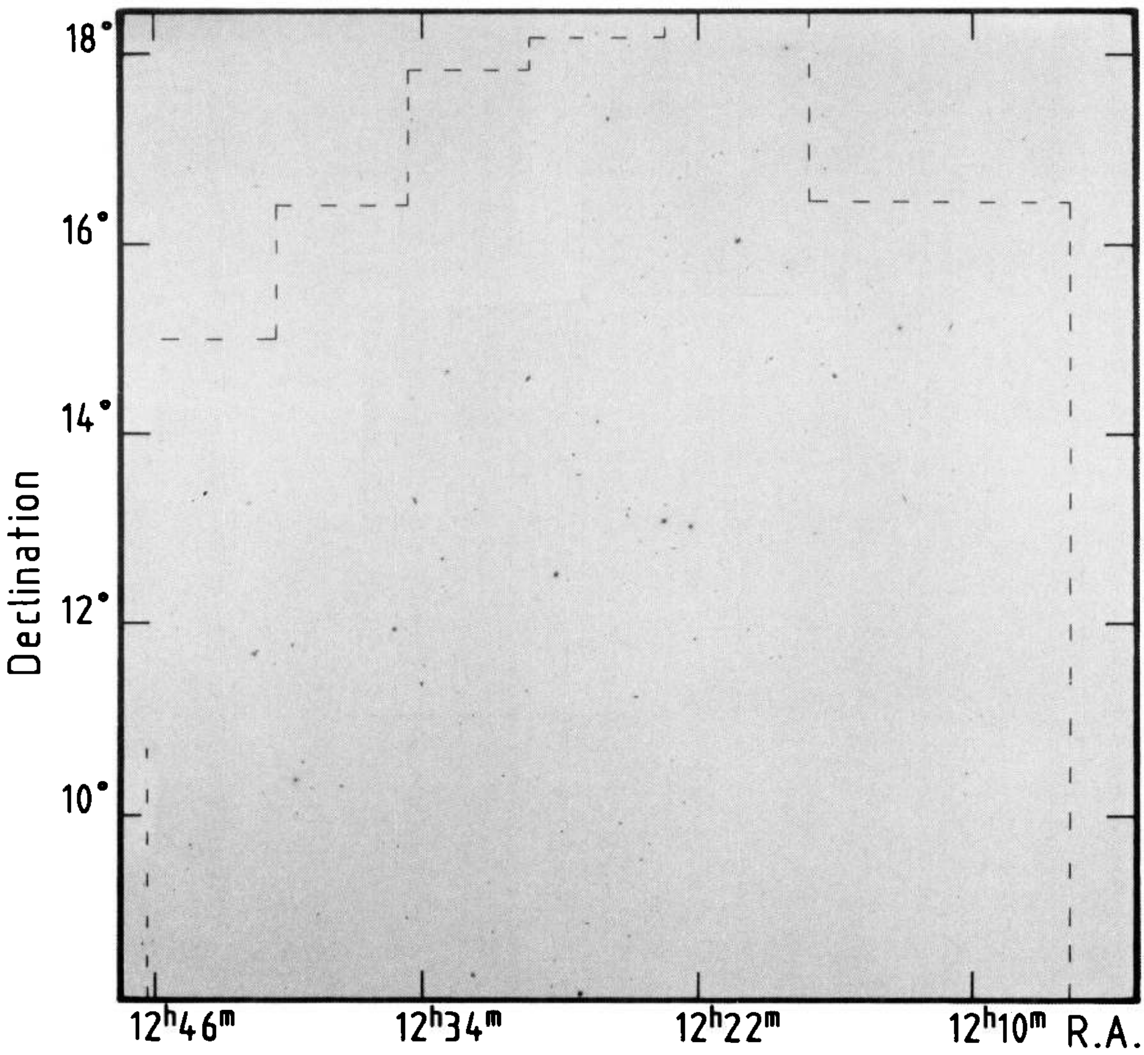

Plate 1. SERC IIIa-J Virgo montage showing the region covered by this work. The dashed lines indicate the area of overlap with the optical catalogue of Binggeli *et al.* (1985).

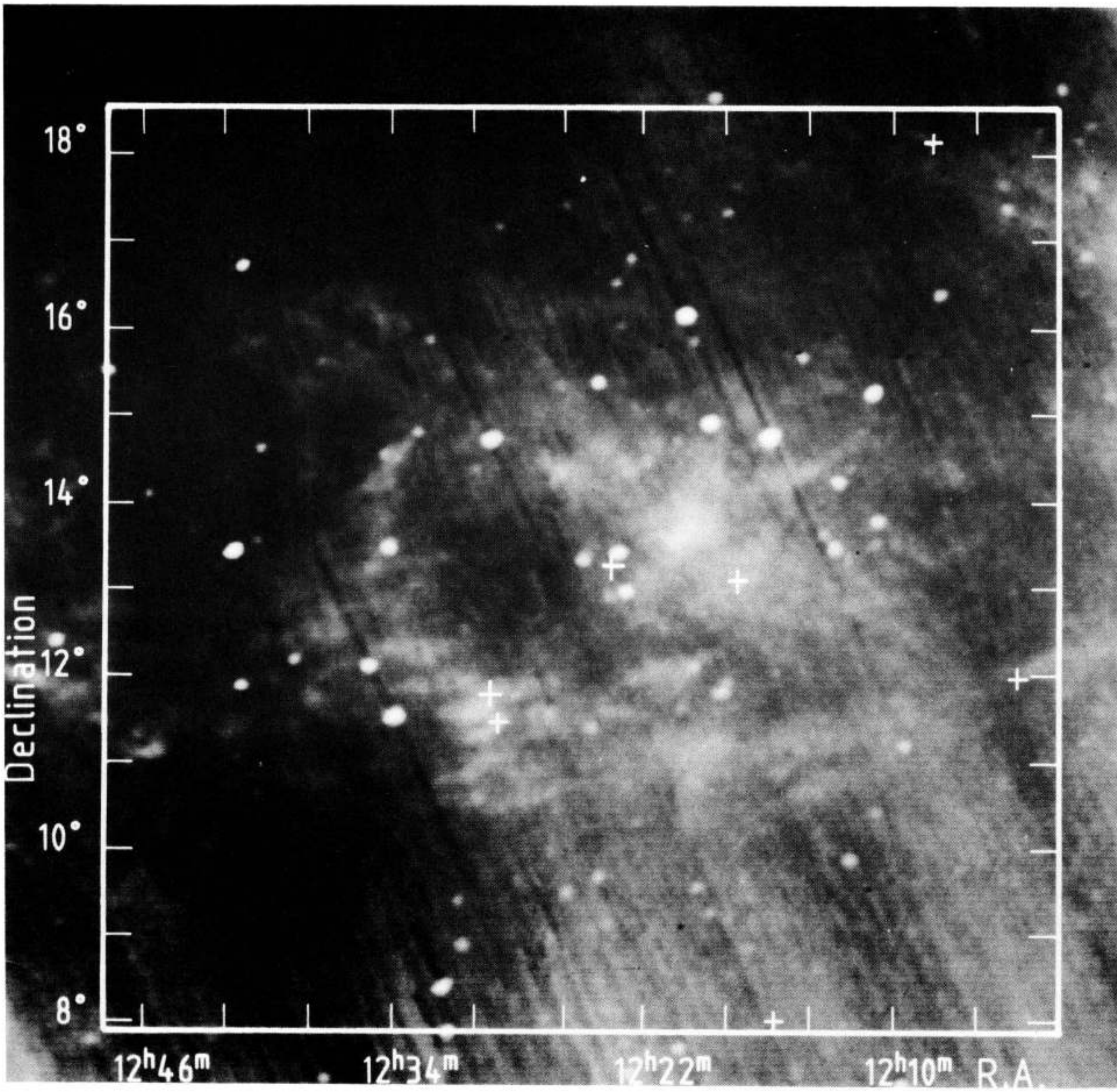

Plate 2. *IRAS* skyflux 100μm image of the Virgo cluster region; the positions of the empty fields found in this work are shown by crosses. Bright *IRAS* galaxies (mainly optically bright spirals, see Plate 1), and infrared cirrus, can be seen.

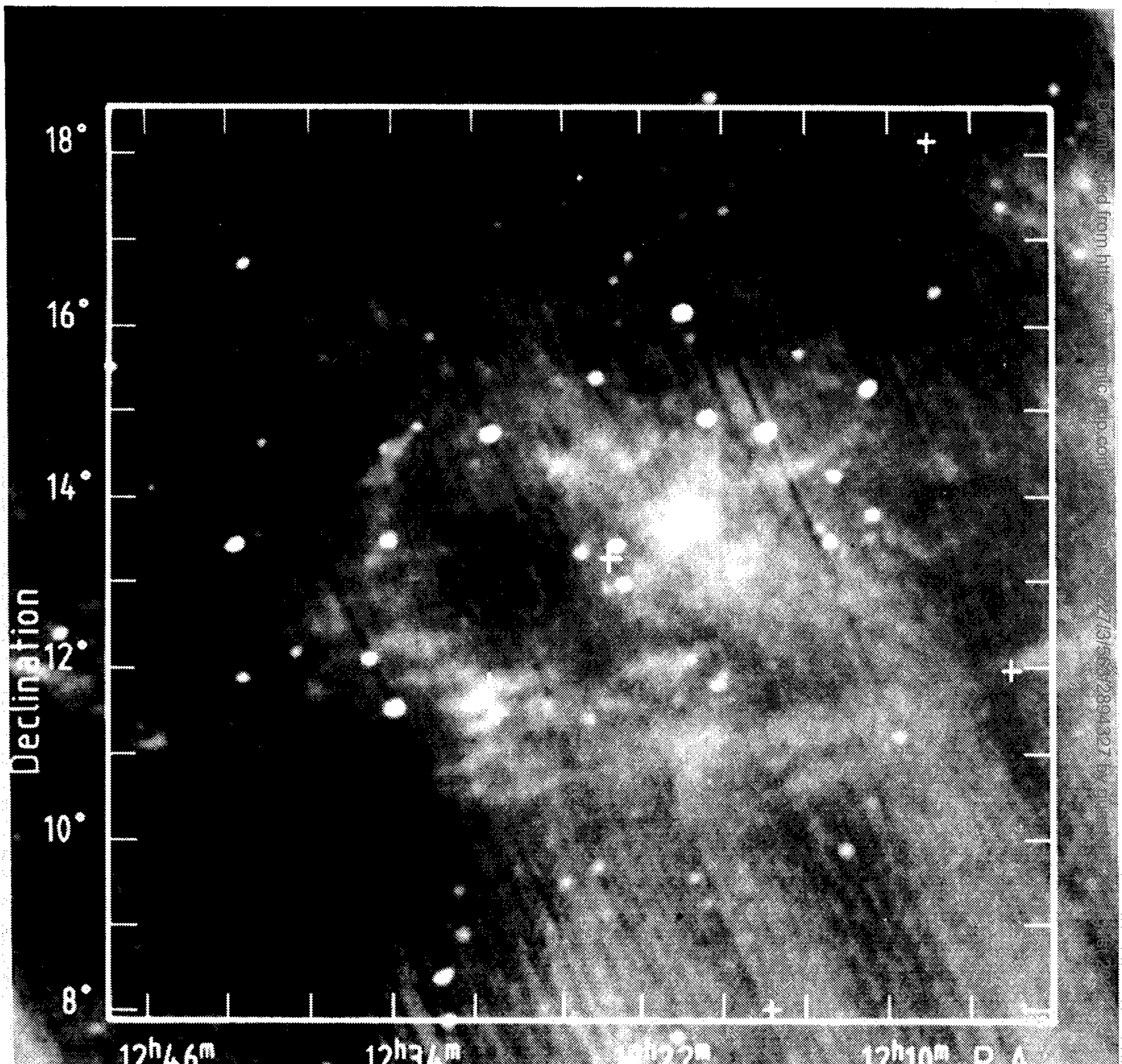

Plate 2. *IRAS* skyflux 100μm image of the Virgo cluster region; the positions of the empty fields found in this work are shown by crosses. Bright *IRAS* galaxies (mainly optically bright spirals, see Plate 1), and infrared cirrus, can be seen.

Column 7: morphological classification: galaxies by eye following de Vaucouleurs (1959); stars from *The Bright Star Catalogue* (Hoffleit 1982) or the SAO catalogue.

Column 8: type code as described in the notes at the end of the table.

Column 9: optical magnitude: galaxies *B*-magnitude either from catalogues or estimated off the plate (see Paper 1); stars *V*-magnitude from catalogues or, for the few uncatalogued stars, *B* estimated from the diffraction spike length on the plate (UKSTU Handbook).

Column 10: B_J magnitude measured by COSMOS for the galaxies.

Columns 11–14: *IRAS* flux densities Jy, not colour corrected; L denotes values that are upper limits only, : denote moderate quality fluxes.

Column 15: logarithm of the ratio of the far-infrared luminosity to the optical luminosity for those galaxies with better than upper limit detections at both 60 and 100μm, and that have COSMOS *B*-magnitudes.

Column 16: logarithm of the far-infrared luminosity in units of solar luminosity for those galaxies that have measured redshifts, and better than upper limit detections at both 60 and 100μm.

Column 17: notes of flags given in the IRPS Catalogue (described at the end of the table); sources are flagged that have nearby extended structure (cirrus and small extended structure), or are themselves extended (poor point source correlation coefficient), those that have nearby point sources (confused), and those that are variable. These are described in detail in the *IRAS* ES. R indicates that there are further remarks at the end of the table.

Plate 3(a)–(g) show finding charts for the optical identifications of the *IRAS* galaxies and empty fields, in RA order. The finding charts are 2×2 arcmin^2 unless otherwise marked. They have been made from UK Schmidt Telescope plate material, apart from one source (12156+0801), on the edge of a IIIa-J plate, which has a finding chart from a Palomar plate.

The IRPS positional errors are approximately Gaussian, with a FWHM of about 20–30 arcsec in both right ascension and declination for this region. The COSMOS measured offsets (optical–*IRAS*) for the stellar sources and the galaxies are plotted in Figs 1 and 2. The semi-major and

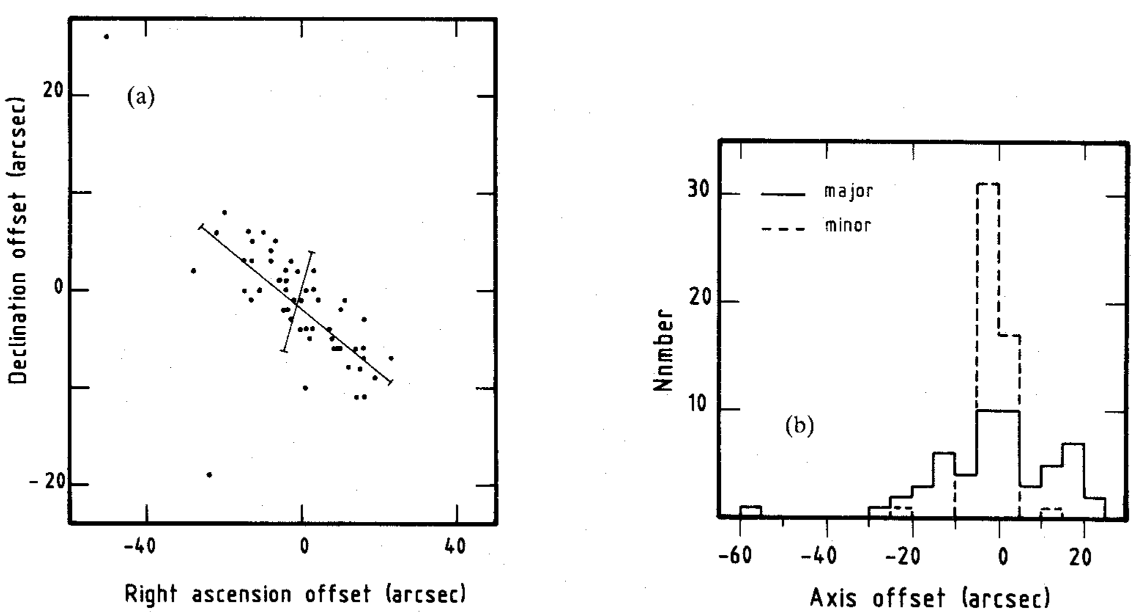

Figure 1. Positional differences between the COSMOS measured optical position and the *IRAS* position for the 54 stellar sources. (a) Plot of declination offset against right ascension offset, arcsec. The bars define the major and minor axes and the 95 per cent confidence error ellipse. For a two-dimensional Gaussian distribution these are equivalent to 2.45σ and equal 27 and 6 arcsec. The bars are not orthogonal because of the different scales of the axes. (b) Histograms showing the offsets (optical–*IRAS*) along the major and minor axes. There is a small offset from $(\Delta\alpha, \Delta\delta)=(0,{}^*0)$, and the *IRAS* positional errors are approximately Gaussian.

1987MNRAS.227..563L

Table 1.

IRAS Name	Optical posn. HHMMSSS	DD'''""	Offset opt-IRPS RA"	Dec"	Name	Type	Type Code	B/V mag.	Cosmag	IRAS Fluxes 12um	25um	60um	100um	log LIR/LB	log LIR, $L_\odot$	Comments
12030+1358	12 2599	135850	-1	0		Sab	6	16.65		0.25L	0.37L	0.89	1.44			EX4
12030+0916	12 3 69	916 2	60	-30	M+02-31-027	galaxy	12	15.00		0.31L	0.37L	0.51L	1.65			CI?EX3; R
12032+1707	12 3143	17 748	-9	0		galaxy	12	20.00		0.25L	0.49L	1.40	1.41			IG?
12041+1759	12 4109	175938	54	-13	M+03-31-039	galaxy	12	14.70		0.29L	0.25L	0.42	1.11			CI?
12041+1158	(12 4 88	115832)				ef/cirrus	14			0.67L	0.58L	0.40L	1.03			CI?EX3, 4
12045+1716	12 4362	171625	8	-5	A1204+17	SA(s):0/a	5	14.85		0.27L	0.59	3.36	7.05			EX2, 3; CI?
12047+1252	12 4485	1252 8	22	-26		S(r):ab	6	17.00		0.38L	0.47L	0.55	1.69			EX3
12048+1709	12 4522	1710 2	-6	6	M+03-31-045	SA(s):c	7	15.50		0.62L	0.27L	0.65	1.25L			CI?EX3
12051+1734	12 5128	173451	42	24	ZG1205+17	galaxy	12	15.50		0.26L	0.28L	0.60	0.96:			CC4
12055+1039	12 5319	103949	-49	12	N4124	SA(s):0	5	12.70		0.25L	0.28L	0.45L	1.47			CI?
12066+1727	12 6401	172748	14	-11	SA099962	K5	2	7.40		3.86	0.95	0.40L	1.00L			EX2
12069+1118	12 6547	1119 2	0	7		galaxy	12	18.70	18.32	0.25L	0.37L	0.48	1.03L			CN?
12072+0827	12 7129	82727	-14	6	SA0119247	Ma	3	9.10		0.65	0.30L	0.40L	1.00L			
12075+1642	12 7351	164215	16	-11	SA099969	K2	2	7.06		1.45	0.44L	0.40L	1.00L			
12076+0942	12 7381	94253	-15	11		galaxy	12	19.50	18.70	0.40L	0.36L	0.99	1.20:	1.70		R
12076+1236	12 7387	123614	9	-2	M+02-31-039	Sab	6	14.85	15.90	0.28L	0.65L	0.49L	1.17			CI?EX3
12080+1618	12 8 45	161840	-4	2	N4152	Sc(r)I4	7	12.46	12.45	0.32:	0.53	4.13	9.20	-0.08	10.2	SB; CC1
12081+1809	(12 8112	18 9 8)				ef/cirrus	14			0.82L	1.00L	0.52L	1.52			CI?EX3; R
12084+0859	12 8285	85946	-3	3	SA0119256	K0	2	8.30		0.58	0.37L	0.40L	1.17L			
12086+1441	12 8412	144115	-4	-11		S:ab	6	16.69	16.68	0.25L	0.48L	1.25	1.71	1.01		CN?R
12086+1809	12 8423	18 958	4	2	ZG1208+18	SA(s):b	6	14.60	14.43	0.25L	0.35L	0.84	1.60	-0.01		CI?EX4
12087+0852	12 8453	85245	23	-7	SA0119258	K0	2	8.50		0.42	0.32L	0.40L	1.02L			
12092+1644	12 9132	164415	-5	4		galaxy	12		17.98	0.25L	0.38L	0.45	1.16:	1.20		EX3
12099+1224	12 9591	1224 8	27	-17	M+02-31-047	S(rs):c	7		13.83	0.25L	0.37L	0.40L	1.28			CI?
12102+1108	1210131	11 839	7	18	N4178	SBc(s)II	11	11.89	12.37	0.25L	0.34L	1.52	8.10	-0.33	9.2	SB; CC3; EX3, 4
12102+1123	1210135	112322	0	-1	SA099986	Ma	3	8.50		2.19	0.56:	0.40L	1.00L			VAR
12106+1634	1210363	163430	-9	6	M+03-31-075	SA0	5	14.80	14.55	0.25L	0.31L	0.63	1.79:	-0.01		
12106+1147	1210411	114739	9	-6	SA099996	K5	2	7.80		1.46	0.42:	0.40L	1.00L			CC2; CI?EX1
12109+1727	1210570	172730	-13	-1	SA099999	K2	2	7.70		0.81	0.61L	0.40L	1.00L			CI
12110+1624	1211 55	162356	9	-9	A1211+16	SB(s):d	11	14.80	13.83	0.40L	0.28L	0.51	1.08L			ARP260
12112+1342	1211146	134216	-2	6	N4189	SBc(sr)II	11	12.53	11.65	0.25L	0.47:	3.23	8.40	-0.48	10.1	SB
12112+1510	1211160	151037	-2	2	N4192	SbII:	6	10.92	10.21	0.33L	0.45L	5.02	18.38	-0.78	9.7	SB; CI?CN; EX1, 3
12113+1326	1211206	1327 1	-40	15	N4193	Sc(s)II	7	13.20	13.55	0.25L	0.27L	1.30:	3.56	-0.10	9.8	SB; CI
12115+1225	1211311	122531	15	-8	SA0100002	K0	2	8.50		0.37	0.94L	0.40L	1.08L			
12118+1445	1211524	144530	18	-13		galaxy	12	20.00	18.70	0.25L	0.28L	0.83	1.43:	1.67		
12119+1831	1211589	183146	-14	-4	ZG1212+18	SA0	5	15.00		0.25L	1.16L	0.66L	1.16			CI
12126+1711	1212410	1711 6	1	-4	SA0100009	K2	2	6.80		0.92	0.47	0.40L	1.01L			
12127+1318	1212441	1318 7	0	6	N4206	Sc(s)	7	12.77	13.36	0.25L	0.40L	0.52	2.48	-0.43	8.7	SB; CI; EX3
12129+0951	1212573	95147	0	2	N4207	Scd sp	7	13.48	14.06	0.54L	0.35L	2.98	7.20	0.44	9.3	SB; CI?
12130+1411	1213 65	141049	55	-22	N4212	c(s)II-III	7	11.86	11.40	0.41L	0.65:	6.57:	16.12	-0.28	9.7	SB; CI?EX1, 2
12133+1325	1213215	132536	-8	-8	N4216	Sb(s)	6	10.97	11.55	0.34L	0.31L	0.93L	7.42			SB; CI; EX3, 4
12138+1334	1213502	1335 9	-8	10	N4222	Scd sp	7	13.91	14.27	0.25L	0.25L	0.92	3.02	0.08	8.9	SB; CI
12138+1110	1213538	111023	4	-4		S:cd	7	17.50	16.74	0.87L	0.30L	0.68	1.05L			EX3
12144+1012	1214267	101217	-7	9	8ZW176	galaxy	12	17.00	17.13	0.70L	0.40L	0.49	0.90:	0.83		CI
12146+1536	1214391	1536 2	6	-1	N4237	Sc(r)II.8	7	12.53	12.16	0.33:	0.71L	2.76	8.86	-0.29	9.4	SB; CC1
12147+1638	1214449	163858	-8	5	M+03-31-093	S:ab	6	15.60	14.76	0.37L	0.30L	0.44:	1.22:	-0.08		CC3; CI?EX3
12149+1254	1214568	125456	-21	9		galaxy	12	17.45	16.51	0.29L	0.40L	0.51	0.92:	0.59		CC4; CI?
12150+1700	1215 52	17 017	3	-8	M+03-31-095	Sc sp	7		14.93	0.87L	0.39L	0.43:	1.11	-0.04		CI?
12151+1525	1215117	152523	4	-1	BS4676	K4III	2	6.34		2.60	0.57L	0.40L	1.00L			
12156+0801	(1215399	8 129)				ef	14			0.29L	0.45L	0.44	1.17L			CI?R
12157+1653	1215483	165324	17	-14		SB(s):d	11	16.60	16.13	0.38L	0.32L	0.52	1.17L			CC3; CI?
12159+0820	1215547	82033	7	-4	SA0119318	K0	2	8.00		0.42	0.35L	0.40L	1.00L			EX1
12161+1200	1216 93	12 028	17	3	M+02-31-085/6	SAb	6		15.87	0.26L	0.30L	0.69:	1.19:	0.46	9.1	CC4; IG?R
12161+1828	1216 96	182819	16	-10	ZG1216+18	S:0/a	5	16.20		0.41L	0.29L	0.65	1.50			
12162+1047	1216146	104749	11	-9		galaxy	12	19.00	18.18	0.40L	0.40L	0.69	1.00L			CI; CN?IG?
12162+1441	1216170	144152	-3	14	N4254	Sc(s)I.3	7	10.43	9.85	1.05	1.36	22.83	71.28	-0.31	10.3	SBVARCICN?EX1-3
12165+1649	1216343	164938	1	-10	SA0100038	G2V	2	7.07		0.30	0.25L	0.72	1.80L			CC1; CI?EX1
12167+1449	1216476	1449 9	2	-5	SA0100039	K0	2	6.53		1.42	0.43L	0.40L	1.00L			
12173+1152	1217192	115234	-4	0	SA0100045	MB	3	8.50		4.71	1.22	0.40L	1.00L			VAR; CI?
12173+0912	1217200	91254	8	-5		S0	5	16.80	16.89	0.27L	0.44L	0.91	1.01L			
12174+1305	(1217293	130512)				ef/cirrus	14			0.25L	0.33L	0.40L	1.34			CI
12175+1733	1217308	173345	-4	-2	SA0100047	star	4	8.20		1.22	0.39L	0.40L	2.88L			CN?EX3
12175+1407	1217326	14 758	-13	5	SA0100048	K0	2	6.94		0.72	0.27L	0.40L	1.00L			
12176+1010	1217356	101014	-20	8	SA0100050	K0	2	7.80		0.82	0.30L	0.40L	1.00L			
12177+1737	1217424	173727	-3	3	M+03-32-003	S0	5	14.30	14.34	0.25L	0.30L	0.90	2.53	0.06	10.8	CN; EX3

12181+1804	1218116	18 4 8	8	-6	BS4697	G8III	2	4.74		5.27	1.21	0.40L	1.00L			
12182+1717	1218152	171736	6	-5	M+03-32+17	SA(s):a	6	15.10	14.75	0.25L	0.44L	2.74	5.14	0.63	11.1	
12182+1549	1218167	154911	3	2	SAO100054	KOIII	2	6.47		1.07	1.17L	0.40L	1.00L			
12185+1154	1218323	115431	1	1		IG	13		16.40	0.25L	0.38L	2.90:	4.01	1.26		CI?IG
12187+1147	1218451	114718	-1	1	N4294	SB(s):c	11	13.20	13.16	0.25L	0.31L	2.70	5.54	0.00	9.3	CI?
12190+1452	1219 52	145240	23	-4	N4298	Sc(s)III	7	12.08	10.66	0.43:	0.52:	4.14	19.15	-0.62		SBCC1VAREX23R
12191+1146	1219 82	114645	-38	22	N4299	Scd(s)III	7	12.86	13.39	0.25L	0.40L	2.52	4.75	0.05	9.2	SB;CI?
12195+0919	1219329	91916	-26	14	N4307	Sbc sp	7	12.79	13.31	0.25L	0.36L	0.83	3.87	-0.26	8.9	SB;EX1
12199+1548	1219592	154852	6	-5	N4312	SA(r):c sp	7		11.86	0.25L	0.32L	2.11	6.05	-0.56	9.2	
12200+1204	1220 57	12 450	-3	11	N4313	Sab	6	12.73	12.93	0.67L	0.26L	1.15	4.29	-0.33	9.0	SB;CI?EX4
12201+0936	1220 94	93636	5	0	N4316	Sbc(sp)	6	13.70	14.14	0.30L	0.38L	1.60	5.49	0.28	9.1	SB
12202+1646	1220152	1646 8	8	-13		galaxy	12	18.00	17.43	0.48L	0.26L	0.87	1.31L			EX3;R
12204+1605	1220229	16 6 9	-27	25	N4321	Sc(s)I	7	10.11	9.25	0.79	1.32	17.98	56.55	-0.65	10.2	SB;VAR;EX1-3
12204+1049	1220251	104929	-10	-2	M-02-32-018	SAb/Pec	6	15.30	15.59	0.25L	0.33L	0.76	1.54	0.42	10.5	
12206+1439	1220401	143958	5	-1	I3244	SA(s):c	7	15.90	14.57	0.36L	0.26L	0.58	1.32	-0.08	9.6	CI?
12207+1138	1220444	113842	-1	-4	N4330	Sd sp	7	13.10	13.56	0.25L	0.36L	0.63	2.78	-0.29	8.6	SB
12210+0955	1221 20	95535	13	2		IG?	13		15.70	0.47L	0.87L	0.59	1.13:	0.34	10.2	CC3;EX1;IG?
12210+1748	1221 59	1749 6	0	9	N4344	SAO	5	13.50	12.77	0.35L	0.25L	0.50:	1.80	-0.76	8.7	CI?
12211+1245	1221117	124517	8	-8	I3258	Sc(s)II.8	7	13.75	14.32	0.42L	0.34L	0.48	0.96:	-0.29	8.5	SB;CC3,4;EX3
12214+1229	1221288	122852	-7	-10	N4351	Sc(s)II.3	7	13.04	13.63	0.26L	0.30L	0.72	1.83:	-0.34	8.7	SB
12217+0848	1221422	84849	0	-2	M+02-32-026	SA(s):cd	6		13.92	0.43L	0.37L	0.59:	1.50	-0.31	8.6	CI
12224+1309	1222314	13 953	24	-7	N4374	E0	5		10.75	0.43L	0.50L	0.50	1.36L			CI?
12228+1017	1222495	101737	23	-8	N4380	SA(r):c	7		12.74	0.57L	0.31L	0.62	3.12	-0.59	8.8	CI?
12228+1644	1222538	164449	12	-2	N4383	SA(s):a	6	13.00	12.61	0.38L	1.04	8.53	11.98	0.22	9.7	EX1-3
12229+1001	1222584	10 145	-10	6	SAO100092	K5	2	8.20		1.12	0.38L	0.40L	1.00L			
12232+1256	1223143	125619	-1	-4	N4388	SA(s):bc	7		12.30	1.00	3.57	10.73	17.27	0.21	9.8	VAR;EX1
12233+1044	1223182	1044 9	3	5	N4390	Sbc(s)II	7	13.27	13.82	0.25L	0.33L	0.80:	1.97	-0.23	8.8	SB;CI?
12234+1829	1223250	182924	-1	1	N4394	SBb(sr)I-	10	11.76		0.30L	0.25L	0.99	4.16			SB
12234+1556	1223280	155648	10	0	N4396	Sc(s)II	7	13.02	12.29	0.81L	0.48L	1.25	3.68	-0.60	9.0	SB
12234+1315	(1223294	131558)				ef?	14			0.47L	0.29L	0.54	1.00L			R
12235+1608	1223314	16 825	-11	0	SAO100095	KO	2	6.73		0.95	0.26L	0.40L	1.00L			
12235+1323	1223352	132320	-3	-4	N4402	Sc (sp)	7	12.56	11.85	0.53:	0.61	5.69	16.94	-0.12	9.7	SB
12235+1627	1223354	162727	13	-4	N4405	Sc(s)/S0	5	12.99	12.52	0.31L	0.25L	1.50	4.52	-0.43	9.6	SB
12239+1001	1223554	10 133	4	-3		galaxy	12	20.00	18.14	0.41L	0.47L	0.51	1.00L			R
12239+1253	1224 1	125314	3	-4	N4413	SBbc(rs)	11	12.97	11.47	0.25L	0.29L	1.01	3.18	-1.01	8.9	SB
12240+0810	1224 4	81013	0	-4	SAO119397	K2	2	8.00		0.50	0.29L	0.40L	1.00L			CI?CN?
12240+1707	1224 13	17 716	-40	14	M+03-32	SB(s):b	10	15.18	14.90	0.25L	0.29L	0.49	1.18	-0.01	9.7	R
12242+0909	1224142	9 945	-3	27	N4411B	Sc(s)II	7	12.92	13.54	0.25L	0.39L	0.42L	1.83			SB;CI?
12242+0811	1224142	81144	13	-3	N4416	SBc(s)II	11	12.89		0.25L	0.44L	0.97	2.79			SB;CI?CN?
12244+1519	1224246	151928	0	1	N4419	SA(s):a	6		11.91	0.55	1.46	7.69	17.32	-0.03	9.7	CI?EX1
12246+0941	1224392	94150	-23	13	N4424	SA(s):ab	6	13.39	12.82	0.25L	0.54L	3.15	5.85	-0.09	9.3	CI?
12249+1123	1224545	112311	2	10	N4429	SA(r):0+	5		10.49	0.33L	0.32L	1.51	4.44	-1.24	9.1	
12249+0817	1224557	81721	16	-7	SAO119407	K2	2	8.30		0.38	0.44L	0.40L	1.19L			
12251+1321	1225 80	132124	6	-1	N4435	E5	5	11.90		0.26L	0.75L	2.04	3.99:			CN?EX3
12251+0853	1225 97	85315	11	-1	BS4741	G8III	2	6.37		0.87	0.36L	0.40L	1.00L			CI?
12252+1317	1225138	1317 6	0	1	N4438	SB(s):a	10	12.00		0.25L	0.26L	4.01	10.44			CN?EX3
12257+1206	1225429	12 610	14	-6	SAO100114	KO	2	8.10		0.58	0.38L	0.40L	1.00L			
12259+1721	1225584	172136	1	-5	N4450	SAB(s):bc	9		11.76	0.25L	0.25L	1.18	6.85	-0.66	9.2	EX3
12260+1223	1226 22	122336	-15	0	SAO100118	KO	2	8.00		0.32	0.42L	0.40L	1.13L			
12260+1702	1226 46	17 242	-13	3	SAO100119	star	4	8.60		1.28	0.39L	0.40L	1.17L			CI?
12260+0932	1226 80	932 8	38	-15	N4451	Sc(s)III	6	13.31	13.25	0.25L	0.37:	1.68	4.32	-0.12	9.1	SB;CI?
12262+1516	1226117	151632	-14	2	I3392	Sc/Sa	6	13.30	13.58	0.25L	0.29L	0.91	3.29	-0.18	8.9	SB;CI?
12264+1415	1226287	1415 9	11	-10	N4459	S0	5	11.60	12.03	0.27L	0.30L	1.72	4.18	-0.61	9.1	CN?
12265+1413	1226340	141335	-4	2	SAO100121	K5	2	8.00		0.68	0.31L	0.40L	1.00L			CN?
12266+1447	1226380	144759	-8	0		galaxy	12	18.00	17.86	0.25L	0.26L	1.03	1.49	1.40		
12268+1641	1226549	164052	20	-9	M+03-32-051	SA(s):a	6	13.90	14.63	0.25L	0.27L	0.59	1.37	-0.05	8.6	EX3
12269+0901	1226556	9 135	2	-2	N4469	S0-a	5	12.60	11.62	0.25L	0.32L	1.14	2.93	-0.94	8.9	
12269+1129	1227 6	112930	21	-7		S0/a	5	15.69	14.89	0.27L	0.38L	0.75	1.69	0.16		CI?
12270+0806	1227 54	8 6 0	7	-3	N4470	S0/a	5	12.90		0.46L	0.35L	1.82	4.31			
12272+1455	1227154	145535	12	-8	SAO100127	KO	2	7.10		0.77	0.49L	0.40L	1.00L			
12274+1237	1227271	123728	17	-7	N4476	E1	5	14.00	13.99	0.25L	0.28L	0.58	1.56	-0.28	8.6	
12275+1354	1227305	135446	-39	18	N4477	SA(r)0	5		12.08	0.35L	0.55L	0.58	1.07	-1.12	8.6	
12276+1810	1227366	181016	3	-4	SAO100132	MB	3	7.50		8.57	2.32	0.51	1.00L			VAR
12282+1240	1228171	124022	22	2	N4486	E0	5		9.01	0.48L	0.34L	0.46	1.15L			EX1,3
12284+1145	1228251	114533	1	4	N4491	SB(s):ab	10		12.89	0.25L	0.50	2.59	3.17	-0.21	9.2	CI;EX4
12286+1653	1228354	165324	-15	3	SAO100135	K2	2	7.70		0.57	0.29L	0.40L	1.00L			
12289+1129	(1228588	112902)				ef/cirrus	14			0.40L	0.32L	0.40L	1.19			CC4CI?EX3,4;R
12291+1707	1229 83	17 742	1	-6	N4498	SBc(s)II	11	12.62	13.32	0.25L	0.29L	1.19	3.70	-0.20	9.0	SB
12293+1524	1229233	152359	7	-4	IC797	SBc(s)II	11	14.01	14.18	0.35L	0.59L	0.95L	2.05			SB;CI
12293+1148	(1229191	114842)				ef/cirrus	14			1.21L	0.32L	0.40L	1.01			CC4;CI;R
12294+1441	1229279	144145	-5	17	N4501	Sbc(s)II	7	10.27	10.95	0.70	0.93	13.96	54.38	-0.02	10.1	SB;CC1,2;EX1-3
12301+1419	1230103	141930	-17	9	I3476	Sc(s)II.2	7	13.29	13.76	0.25L	0.31L	1.29	3.03	-0.05	9.0	SB;EX3
12305+1034	1230309	103418	3	0	BS4777	G8III	2	6.26		0.91	0.77L	0.40L	1.00L			CI
12306+0806	1230380	8 635	1	-2	[illegible]	[illegible]	10	[illegible]		0.44L	[illegible]	[illegible]	1.00L			CI?R

Table 1–*continued*

IRAS Name	Optical posn. HHMMSSS	DD''"	Offset opt-IRPS RA"	Dec"	Name	Type	Type Code	B/V mag.	Cosmag	IRAS Fluxes 12um	25um	60um	100um	log LIR/LB	log LIR, L⊙	Comments
12307+1231	1230420	123121	-11	0	M+02-32-130	SB:a	10	14.90	14.71	0.40L	0.29L	0.84	1.76	0.12	10.6	CI?
12307+1621	1230451	162138	1	4		galaxy	12	17.40	17.14	0.25L	0.25L	1.14	1.30	1.12		CN?
12307+1648	1230481	164821	8	-5	DO14603	star	3	14.50	15.71	0.93	1.09L	0.40L	1.00L			
12308+0856	1230578	85549	62	-23	N4519	SBc(rs)II	11	12.34	11.78	0.36L	0.68	3.71:	5.78	-0.46	9.3	SB; CI?CN?
12311+0926	1231 74	92658	-10	0	N4522	Sc/Sb	7	12.73	12.28	0.25L	0.32L	1.29	3.89	-0.59	9.0	SB; EX3
12313+1526	1231170	152638	-30	-4	N4523	SBd(s)III	11	13.62		0.25L	0.58L	0.38:	1.31			SB; CI
12316+1614	1231392	161438	25	-9	M+03-32-070	SB(s):c	11		15.72	0.25L	0.30L	0.51	1.27:	0.34	9.8	CI?
12317+1321	1231444	1321 3	-14	1	N4531	SB(r):0	5	12.30	11.66	1.72L	0.51L	0.40L	1.55			CI
12318+0828	1231480	828 8	-4	-8	N4535	SBc(s)I.3	11	10.51		0.25L	0.70L	6.42	20.88			SB; CI; CN?EX1-4
12319+0800	1231582	8 039	-2	-1	SAO119479	K2	2	6.70		0.84	0.27L	0.40L	1.00L			CI?
12321+0916	1232113	91648	-3	-6	M+02-32-144	SO	5	15.80	15.40	0.28L	0.29L	0.81	1.49	0.35	9.7	CC3
12322+1331	1232181	133150	21	-10		galaxy	12	15.87	16.99	0.49L	0.25L	0.46	1.10L			
12323+1549	1232198	154933	-20	-8	N4540	Scd(s)III	7	12.49	13.20	0.29L	0.46L	1.33:	5.51	-0.13	9.1	SB; CI?EX3
12328+1446	1232554	144611	27	-2	N4548	SBb(rs)I	10	11.12	11.56	1.82L	0.25L	1.21	7.76	-0.70	9.2	SB; CI?EX3, 4
12330+1554	1233 22	155442	-7	5	SAO100163	K5	2	8.00		0.60	0.25L	0.40L	1.00L			CI
12332+1156	1233 96	115632	-42	5		SB(r):0	5	15.50	15.12	0.25L	0.31L	0.60	1.17:	0.12		CI; CN?
12340+1130	1234 16	113119	-11	24	N4568/7	Sc(s)III	7	11.70	10.58	0.58	0.98	15.31:	46.61	-0.19	10.1	SB; CI; EX1-3
12341+1332	1234126	133212	21	6	I3583	SmIII	7	13.91	12.61	0.43L	0.35L	0.60	1.88L			SB; CI; CN?EX1, 2
12343+1326	1234186	132619	8	-3	N4569	Sab(s)I	6	10.25	10.94	0.35L	0.89	7.08	22.72	-0.37	9.8	SB; CI?CN?EX1-3
12344+1429	1234261	142949	7	23	N4571	Sc(s)II	7	11.81	12.20	0.25L	0.25L	0.94	6.28	-0.54	9.1	SB; CI?EX1, 3
12344+1721	1234279	172150	-5	-2	BS4801	K5III	2	5.68		5.03	1.19	0.40L	1.15L			
12345+1828	1234314	182838	1	3		galaxy	12	17.80		0.36L	0.33L	0.93	1.30			
12350+1149	1235 63	1149 2	27	-9		galaxy	12	17.00	17.19	0.27L	0.38L	0.58	1.00L			CI; EX1
12350+1051	1235 64	105133	19	-9	SAO100181	K2	2	8.20		0.77	0.29L	0.40L	1.00L			
12351+1205	1235117	12 534	1	-3	N4579	Sab(s)II	6	10.56	9.92	0.38L	0.33L	4.46:	17.38	-0.93	9.6	SB; CI; EX1-3
12355+1724	1235323	172342	4	-19		galaxy	12	17.00		0.36L	0.36L	0.69	1.18L			CN?EX4; IG?
12360+1404	1236 40	14 451	16	-6	SAO100187	KO	2	7.20		0.62	0.37L	0.40L	1.00L			CI?CN?
12363+1404	1236205	14 443	1	0	SAO100189	Mb	3	8.50		10.74	5.01	0.68	1.00L			CI?CN?
12371+1651	1237 66	165145	7	10	M+03-32-080	IRR	12		15.99	0.25L	0.64L	0.66:	1.30	0.51		CI?
12371+0841	1237 75	84151	-28	1		SO	5		16.34	0.25L	0.29L	0.58	1.07:	0.59		
12373+1534	1237210	153419	-5	2	N4595	Sc(s)II.8	7	12.92	13.65	0.25L	0.43L	0.92	2.88	-0.18	8.9	SB
12377+0848	1237421	848 7	-8	3	SAO119523	G5	2	8.50		0.31	0.31L	0.40L	1.08L			
12382+1259	1238127	125925	10	-2	SAO100203	K2	2	8.00		0.99	0.27L	0.40L	1.00L			CI?
12384+1211	1238263	1211 9	20	-5	N4606	S:a?	6		12.05	0.40L	0.53L	0.79	2.24	-0.91	8.8	CN?EX3
12385+1539	1238356	153911	-1	2	SAO100205	K2	2	7.80		0.43	0.53L	0.40L	1.00L			
12386+1209	1238410	12 935	14	-11	N4607	Scd sp	7	13.75	12.93	0.38L	0.43L	2.71	7.55	-0.03	9.3	SB; CN?EX3
12389+0908	1238557	9 846	26	-14		galaxy	12		16.86	0.38L	0.42L	0.46	1.00L			CC3; CI?R
12394+1030	1239214	103041	-50	26	BS4828	AOV	1	4.88		0.62	0.56L	0.40L	1.00L			
12395+1425	1239317	1426 1	-8	4	SAO100212	star	4	8.60		1.46	0.45	0.40L	1.09L			VAR; CI
12401+1434	1240103	1434 8	4	-3	N4634	Sc	7	13.19	13.66	0.43L	0.41L	4.00	10.57	0.42	9.5	SB; CI; CN?EX1
12402+1037	1240176	103753	11	-2	ZG1240+10	S:a	6	14.95	14.91	0.25L	0.32L	1.42	2.08	0.36	10.7	
12402+1338	1240187	133758	29	-6		galaxy	12	16.60	18.01	0.32L	0.27L	0.36	1.25L			CN?
12403+1331	1240214	133152	8	0	N4639	SBb(r)II	10	12.19	12.81	0.25L	0.31L	1.39	4.36	-0.34	9.1	SB; CN?
12407+1022	1240442	102230	10	-6	SAO100222	MO	2	8.00		3.57	1.06:	0.40L	1.39L			VAR; CI?
12408+1128	1240504	112837	2	1	M+02-32-193	SO	5		16.03	0.40L	0.31L	0.69	1.28:	0.54		CC4; CI?CN?EX3
12410+1151	1241 12	1151 0	4	-20	N4647	Sc(rs)III	7	12.03		0.41	0.56:	4.93	15.28			SB; CI?CN?EX1, 2
12412+1639	1241124	1640 2	-7	3	N4651	SA(s):bc	7		12.30	0.40	0.41	5.15	15.07	0.01		EX1, 2
12412+1102	1241142	11 238	8	0	ZG1241+11	SB(s):b	10	14.50	13.98	0.25L	0.30L	1.19	2.79	0.00	10.8	
12414+1324	1241263	132351	15	-17	N4654	SBc(rs)II	11	11.14	10.50	0.86	1.32	12.96	34.42	-0.33	10.0	SB; VAR; EX1, 2
12426+1003	1242376	10 3 8	20	4		galaxy	12	16.90	16.39	0.38L	0.50L	1.16	1.74:	0.87		CI?CN?EX2, 3
12428+1747	1242510	174739	-6	1	DO14636	star	4	14.50		0.52	0.43L	0.40L	1.00L			EX1
12432+1558	1243145	155813	-5	-5		IG	13	18.00	17.14	0.34L	0.27L	0.54:	1.14	0.90		CI?EX3; IG
12438+0948	1243496	94832	-24	-19	SAO119580	KO	2	5.80		2.19	0.52:	0.40L	1.05L			CI?
12440+1314	1244 57	1314 9	-3	-3	SAO100257	K5	2	8.50		0.81	0.38L	0.40L	1.00L			CI?
12441+1650	1244 85	165057	-28	2	BS4851	K3III	2	5.12		6.73	1.68	0.45L	1.00L			
12445+0920	1244302	92016	-4	1	SAO119586	KO	2	6.86		1.46	0.47:	0.40L	1.17L			
12446+1551	1244402	155151	-3	-3	SAO100259	KO	2	6.64		0.72	0.50L	0.40L	1.00L			CI?
12452+1402	1245150	14 2 6	6	-1	N4689	Sc(s)II.3	7	11.55		0.47L	0.45L	2.65	9.67			SB
12452+1723	1245167	1723 9	16	-3		star	4	14.00		0.37	0.30L	0.40L	1.00L			EX1
12457+1115	1245440	111521	4	-4	N4694	SA(s):a	6		12.08	0.25L	0.45L	1.20	2.74	-0.76	8.9	CI
12458+0845	1245513	84541	11	0	N4698	SB(r):0	5		11.30	0.25L	0.31L	0.47L	1.75			CI?EX3
12460+0923	1246 29	924 3	-4	5		SAa	6		15.10	0.72L	0.45L	0.69	1.27	0.16		
12463+1335	1246175	133544	-22	6	SAO100276	K2	2	8.20		0.63	0.49L	0.40L	1.36L			
12468+1005	1246515	10 516	0	0	ZG1246+10	SAa	6	15.60		0.25L	0.30L	0.39	0.86:			CC4

Notes

Many of these galaxies appear in Sandage, Binggeli & Tammann (1985) where better finding charts are given. Such galaxies are indicated by 'SB' in the last column. The IRPS flags given in the Notes column are abbreviated as follows (a full description is given in the *IRAS* ES): CC(1–4), poor point source correlation for band (1–4) (cc<96 per cent); CI, CI? cirrus flagged (CII>1, CI1=1); CN, CN? confusion flagged (pnearh/m>1, pnearh/m=1); EX(1–4), extended structure in band (1–4) (SES>0); VAR, likely to be variable (VAR>10 per cent). Also noted: IG, IG? interacting galaxy, possible interacting galaxy based on optical morphology.

The type code is as follows:

1 early-type stars (A–F);
2 late-type stars (G–M);
3 extreme M. carbon or Mira stars;
4 faint unclassified stars;
5 elliptical or lenticular galaxies;
6 SA a–b galaxies;
7 SA bc– galaxies;
8 SX a–b galaxies;
9 SX bc– galaxies;
10 SB a–b galaxies;
11 SB bc– galaxies;
12 unclassified galaxies;
13 interacting galaxies;
14 empty fields.

Remarks

12030+0916: Bright galaxy west and south of *IRAS* position has $LR=0.1$. Claimed galaxy SSE of *IRAS* position has $LR=0.3$.
12041+1158: Cirrus, see Plate 2.
12081+1809: Two 15th mag galaxies 1 and 1.5 arcmin off north-west. Closer fainter galaxy to NW could be identification with $LR=1.5$, but cirrus is flagged (and see Plate 2).
12086+1441: Pair of galaxies separated by 30 arcmin. Claimed brighter galaxy which is nearer *IRAS* position and has $LR=34$, *cf.* $LR=27$ for other galaxy.
12092+1644: *IRAS* fluxes consistent with galaxy identification. Nearest object (claimed) looks stellar – possible QSO – $LR=38$. There are some very faint (22nd mag) objects just visible on finding chart with $LR=7$, and implied $L(\mathrm{IR})/L(B)\sim 90$.
12156+0801: On edge of *J*-plate. Also empty on adjoining Palomar O. Objects on Palomar E are flaws. CCD image of very faint object ~40 arcsec east, with $LR\sim 0.5$ and implied $L(\mathrm{IR})/L(B)\geqslant 50$, shows it to be a galaxy. Region seems clear of cirrus.
12161+1200: Peculiar morphological structure. See finding chart.
12165+1649: Fluxes are inconsistent with stellar only identification. Star may obscure a galaxy.
12174+1305: Cirrus, see Plate 2.
12190+1452: *IRAS* position coincident with face on spiral NGC 4298 (see finding chart).
12202+1646: Two faint objects of unknown morphological type in error in box, $LR\sim 22$. Brighter galaxy (17.5 mag) just outside box is claimed, $LR=34$.
12234+1315: Star (unknown) is very close to position. Fluxes do not confirm this identification. NGC 4406 is 7 arcmin south-east. Another 16th mag galaxy is 2 arcmin due south, neither of these are likely ($LR\ll 1$). Star image may obscure faint galaxy. Region seems clear of cirrus, see Plate 2.
12239+1001: Close star and faint galaxy on position. Cosmag will be for the pair combined.
12240+1707: Bright galaxy $LR=42$.
12289+1129: Cirrus 17th mag object 45 arcsec south-east is a star. See Plate 2.
12293+1148: Cirrus. See Plate 2.
12389+0908: Object claimed as identification may be a compact galaxy or a star superimposed on a faint galaxy.

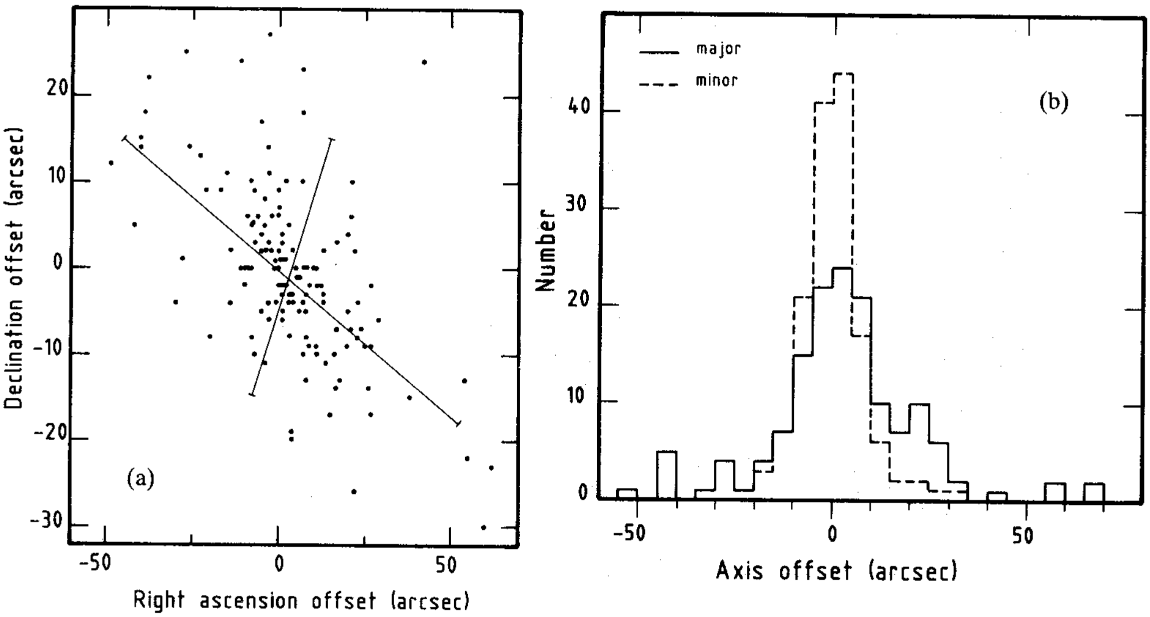

Figure 2. Positional differences between the COSMOS measured optical position and the *IRAS* position for the 145 galaxy sources. (a) Plot of declination offset against right ascension offset, arcsec. The bars define the major and minor axes and the 95 per cent confidence error ellipse. For a two-dimensional Gaussian distribution these are equivalent to 2.45σ and equal 54 and 18 arcsec. The bars are not orthogonal because of the different scales of the axes. (b) Histograms showing the offsets (optical–IRAS) along the major and minor axes. There is a small offset from $(\Delta\alpha, \delta)=(0,0)$, and the *IRAS* positional errors are approximately Gaussian.

semi-minor axes of the 95 per cent confidence error ellipses (2.45σ for two-dimensional Gaussian distributions) are 27×6 arcsec^2 for stars and 54×18 arcsec^2 for galaxies, with the major axes at a position angle of 108°. These compare with 35×7 arcsec^2 for stars and 45×12 arcsec^2 for the fainter (more point-like) galaxies in the SGP area presented in Paper 1 (position angle 66°). The error ellipses are offset from $(\Delta\alpha, \Delta\delta)=0, 0$ by 1–4 arcsec (see Figs 1 and 2); a similar offset was found in Paper 1, although not in the same direction. This offset is probably not significant.

In Paper 1 these two-dimensional Gaussian position errors were combined with the probability of chance coincidence to determine likelihood ratios for our identifications. The likelihood ratio, *LR*, is given by

$$LR=\frac{dp\ (\mathrm{id})}{dp\ (\mathrm{unrelated\ object})}=\frac{Qr\exp(-r^2/2)\,dr}{2\pi r\sigma_J\sigma_N N(B_J)\,dr}=\frac{Q\exp(-r^2/2)}{2\pi\sigma_J\sigma_N N(B_J)}$$

where, Q is the *a priori* probability that an optical identification exists above the survey limit; σ_J and σ_N are the 1σ position errors along the major (J) and minor (N) axes of the ellipse; $N(B_J)$ is the surface density of optical candidates of magnitude B_J or brighter; and r is given by

$$r^2=\left(\frac{\Delta\theta_J}{\sigma_J}\right)^2+\left(\frac{\Delta\theta_N}{\sigma_N}\right)^2,$$

where $\Delta\theta$ is the positional displacement. Following the analysis of Paper 1, Q can be shown to be effectively unity.

The adoption of a particular value of *LR* as acceptable is necessarily a compromise between completeness (low *LR*), and reliability (high *LR*). We adopt $LR>3$ as acceptable, which corresponds to a reliability of 75 per cent for an individual object in the worse case (although the majority of the identifications will have a reliability >90 per cent). Even in this area with a high density of galaxies, sources with $B<17$ can be offset by 2.5σ (~55 arcsec along the major axis) and

Table 2. Number of stars plus galaxies per square degree brighter than B_J at the centre of the Virgo cluster.

B_J	21	20	19	18	17
$N(B_J)$	1425	967	633	385	175

still have an acceptable LR. Table 2 gives the number counts of stars and galaxies for this region, measured off the Schmidt plates. Values of LR have been calculated for some of the more difficult identifications, and are given in the Remarks at the end of Table 1. [These values have been calculated using $N(B_J)$ for stars and galaxies, which is appropriate for an optical point source; however this will result in pessimistic values of LR for the cases where $N(B_J)$ for galaxies only is appropriate.]

Late-type stars and spiral galaxies dominate the *IRAS* detections. Each of our optical sources has been given a type code, described at the end of Table 1, and Fig. 3 shows the population of each category. The properties of the empty fields, stars and galaxies are discussed in detail in the following sections.

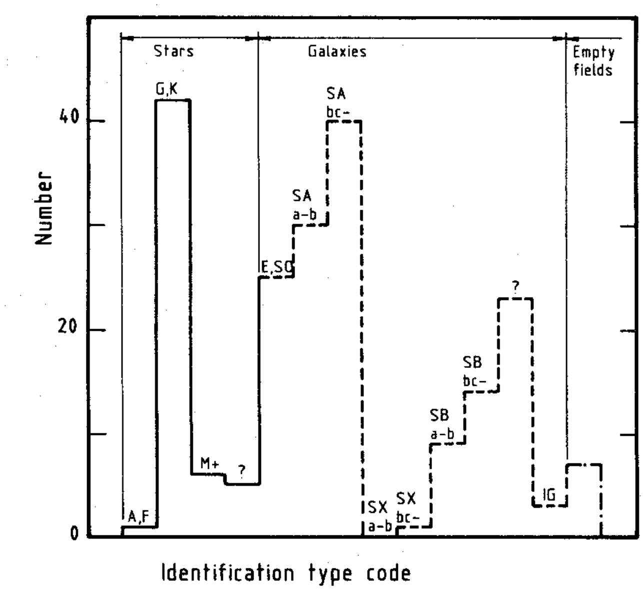

Figure 3. The population of each type of identification, by code described at end of Table 1.

3 Empty fields

Seven *IRAS* sources have no obvious optical counterpart. Table 3 gives a summary of the *IRAS* data for these sources.

Sources 12041+1158, 12174+1305, 12289+1129 and 12293+1148 are completely empty within 1 arcmin of the IRPS position, but have cirrus flagged and can be seen to be in a badly affected area from Plate 2. All these sources are detected at 100μm only.

12081+1809 does have two 15th magnitude galaxies 1 and 1.5 arcmin off NW with $LR \leqslant 1.5$ but cirrus is flagged and visible on Plate 2. This is also a 100μm only source.

The source 12156+0801 is on the edge of the *J*-plate and the objects visible on the Palomar E finding chart in Plate 3 are flaws. There is a very faint object ~40 arcsec east with low LR (~0.5) and high implied $L(\mathrm{IR})/L(B)$ ($\gtrsim$50). A CCD image kindly obtained with the 0.75-m telescope at SAAO by Dr J. Menzies indicates that this object is a disturbed galaxy. The region appears to be clear of cirrus. This is a 60μm only *IRAS* source. The source 12234+1315 has an uncatalogued

Table 3. Empty fields. If no value is given for an IRPS flag, that value is zero. See the *IRAS Explanatory Supplement* (Beichman *et al.* 1985) for a detailed description of the flag (brief descriptions are given in the text).

IRAS NAME	FLUXES, JY 12μm	25μm	60μm	100μm	IRPS FLAGS	REMARKS
12041+1158	0.6697L	0.5843L	0.399L	1.028	CC(4)=D, S1(3,4)=1,2 C1=1,C2=5	Cirrus, see Plate 2.
12081+1809	0.8175L	0.9975L	0.5157L	1.52	CC(4)=B, S1(3)=2, C1=1,C2=4	Two 15th mag. galaxies NW. Closer has LR=1.5, but cirrus flagged and seen on Plate 2.
12156+0801	0.2853L	0.4514L	0.4423	1.17 L	CC(3)=C, C1=1,C2=1	Very faint object ~40" E with LR~0.5 and implied L(IR)/L(B)⩾50. No cirrus seen on Plate 2.
12174+1305	0.2506L	0.3327L	0.4003L	1.335	CC(4)=B, C1=2,C2=5	Cirrus, see Plate 2.
12234+1315	0.4653L	0.2899L	0.5354	1.001L	CC(3)=D, C1=0,C2=3	Star close to position but fluxes not appropriate. Star may obscure faint galaxy. No cirrus seen on plate 2.
12289+1129	0.4042L	0.3171L	0.4002L	1.193	CC(4)=E, S1(3,4)=1,2	Cirrus. Object 45" SE is a star. See Plate 2.

star very close to the *IRAS* position, but the 60 μm flux detection would not support this identification. NGC 4406 is 7 arcmin south-east and another 16th magnitude galaxy is 2 arcmin due south; neither of these is a likely identification ($LR \leqslant 1$). The star image may obscure a faint galaxy. The region seems clear of cirrus, as can be seen from Plate 2.

12156+0801 and 12234+1315 may be genuine empty field candidates. Both of these are 60 μm only *IRAS* sources, suggestive of 'hot' galaxies which are extremely infrared luminous. In Section 5.1.2 it is shown that if *IRAS* galaxies exist that are fainter in the optical than the plate limit ($B>22$), the implied far-infrared luminosity is $\sim 10^{13} L_{\odot}$.

4 Stellar sources

The density of stars detected by *IRAS* in this area (close to the North Galactic Pole with latitude about 80°) is 0.48 per square degree, *cf.* 0.49 at the SGP (Paper 1). Fig. 4 shows a histogram of the *V*-magnitudes for the 54 stars in this sample. The distribution is similar to that at the SGP, showing a steady increase from $V=5$ to $V=8$, and then a sharp drop with a few objects having $V\sim 15$. The star counts given in Allen (1973) for this latitude imply that *IRAS* detected all stars brighter than $V=8$, although the early-type stars have to be brighter at *V* to be detected by *IRAS* at 12 μm.

A colour relation can be used to derive either the maximum *V*-magnitude for detection by *IRAS* at 12 μm, or the expected *IRAS* flux for a given *V*, as a function of spectral type. Waters, Cote & Aumann (1987) have established a well-defined $B-V$: $V-[12]$ relationship for $\sim$6000 bright stars in IRPS, for $-0.25<B-V<1.60$ (approximately B2 to M0 spectral types). Their relationship can be written

$$V-[12]=fn(B-V)$$

so that for a constant $B-V$, i.e. for a given spectral type,

$$V=-2.5\log F(12\,\mu\mathrm{m})+K,$$

where K is a constant. At the lower limit of detection $F(12\,\mu\mathrm{m})=0.3$ Jy, so that

$$V_{max}=1.31+K.$$

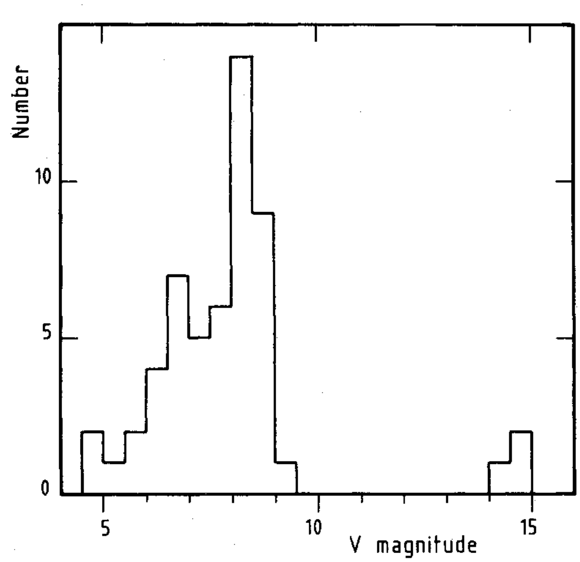

Figure 4. The distribution of *V*-magnitudes for the 54 stellar sources.

Table 4. The value of K, as a function of $B-V$, for the stellar V: $F(12\mu m)$ relation, $V=-2.51 \log F(12\mu m) + K$, and maximum value of V for detection, V_{max}.

B-V	Spectral type	K	V_{max}
0.00	A0V	4.08	5.39
0.27	F0V	4.84	6.15
0.58	G0V	5.55	6.86
0.65	G0III	5.69	7.00
0.89	K0V	6.17	7.48
1.07	K0III	6.55	7.86
1.45	M0V	7.56	8.87
1.60	M0III	8.22	9.53

Table 4 gives values of K as a function of $B-V$, and also gives V_{max}.

Fig. 5 is a plot of the logarithm of the $12\mu m$ flux density (not colour corrected, see *IRAS* ES) against visual magnitude. The V–[12] relationships found by Waters *et al.* for different spectral types are illustrated, and a 2000 K blackbody line is also given. K-type stars are dominant in this sample, as they are in optical (all sky) samples for $V<8$ (Allen 1973). The maximum V-magnitude for *IRAS* detection for K-types is about 8, and this explains the peak in the V distribution shown in Fig. 4.

If the spectral type is known, the $B-V$: V–[12] relation allows any $12\mu m$ excess to be determined. Fig. 5 shows that this sample contains some red giants with infrared excesses (that are probably undergoing mass loss) and some Mira-like stars.

Fig. 6 is a histogram of the ratio of the $12\mu m$ flux density to the $25\mu m$ flux density, for the 14 stars that have moderate- or high-quality detections at both these bands. The majority of the stars have a flux distribution at these wavelengths similar to the Rayleigh–Jeans region of a blackbody [$F(12\mu m)/F(25\mu m) \sim 4$] but again there is evidence of flux excesses at longer wavelengths in some stars, i.e. $F(12\mu m)/F(25\mu m)<4$. Paper 1 showed a similar range (2–4.5) with a sharper peak at 3.5–4.5 for a larger sample of 43 stars. Olnon *et al.* (1984) plotted $F(60)/F(25)$ against $F(25)/F(12)$ for 40 evolved stars in the catalogue and found a well-defined sequence from classical Miras to OH/IR stars. Their values of $F(12)/F(25)$ ranged from 0.05 (OH/IR) to 3.0 (Mira), corresponding to blackbody temperatures of 120–4000 K; comparing this with Fig. 6 confirms that this area of sky contains sources at the Mira end of this sequence [$F(12\mu m)/F(25\mu m) \sim 2$–3].

5 Galaxy sources

5.1 PROPERTIES OF THE VIRGO *IRAS* GALAXIES

5.1.1 The IRPS data

A histogram of the B-magnitudes for the 145 galaxies in this sample is given in Fig. 7; it shows a range of 9 to 20, peaking at $B=12$. The magnitudes used in Fig. 7 are a combination of magnitudes measured by COSMOS ('cosmag') and catalogue values, or, in a very few cases, magnitudes

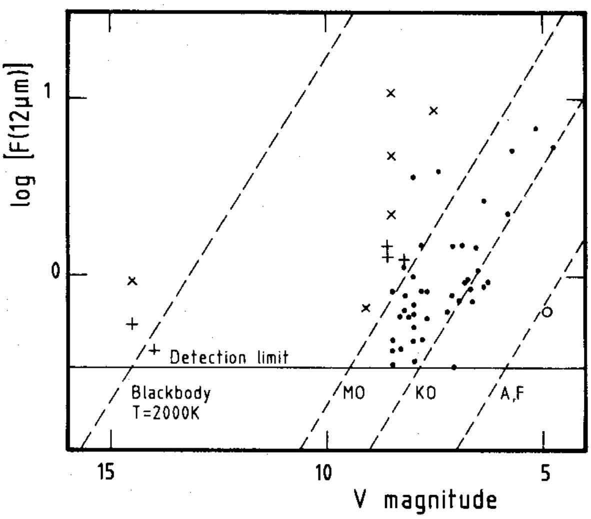

Figure 5. Plot of log [F(12μm)], not colour corrected, against V-magnitude for the 54 stellar sources. The lines show an empirical V: [12] relationship as a function of spectral type (or B–V, see Table 4) and the relation derived for a blackbody with T=2000 K. The symbols distinguish the stars by type code as follows: ○, early-type stars (A, F); ·, late-type stars (G–M); ×, late M, carbon or Mira types; +, optically faint unclassified stars.

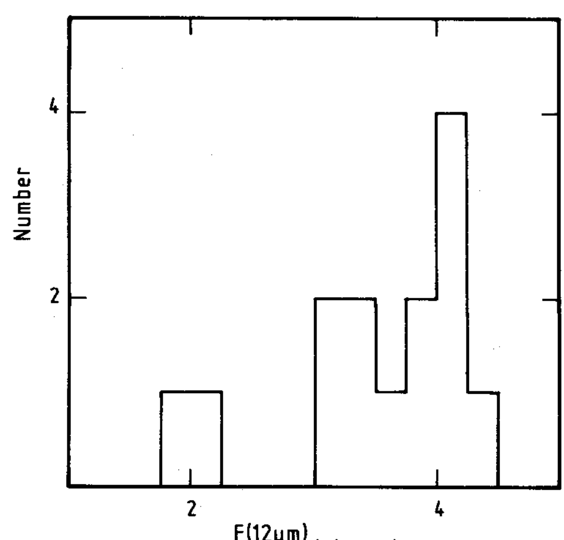

Figure 6. Distribution of the flux density ratio $F(12\mu m)/F(25\mu m)$, neither colour corrected, for the 14 stars with moderate or high-quality detections at both these bands.

estimated off the plate by eye (see Paper 1). Fig. 8 plots this other B-magnitude against 'cosmag' and shows deviations of up to a magnitude, with a mean difference of 0.6 magnitudes. These deviations reflect mainly the error in the catalogue and estimated B-magnitude, and the dispersion within that group; the relative error in the cosmag is about 0.2 mag, with a zero-point uncertainty of $\leq$0.5 mag. In the following analyses we will use the 119 galaxies with COSMOS magnitudes to define a homogeneous sample.

Fig. 9 is a histogram of the values of log [L(IR)/L(B)] for the 97 galaxies with cosmags and better than upper limit detections at both 60 and 100 μm. The parameter L(IR) is a measure of the flux emitted from 42 to 122 μm (in W m^{-2}, see Lonsdale *et al.* 1985 where it is defined as FIR), such

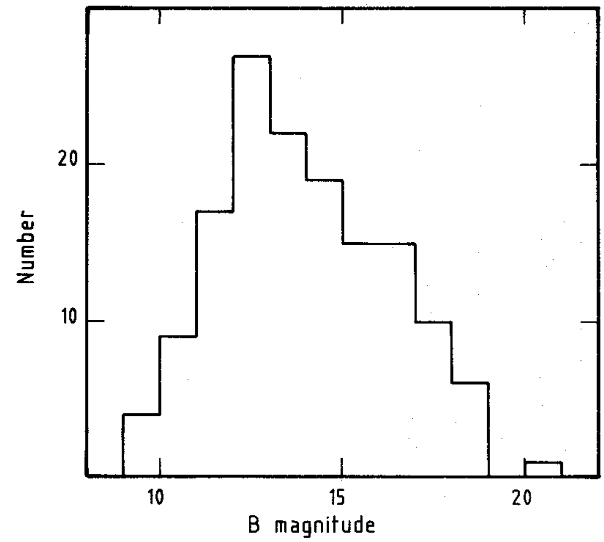

Figure 7. Distribution of the B-magnitudes for the 145 galaxy sources. The magnitude source is predominantly COSMOS, although catalogues and plate estimates by eye have been used for 26 galaxies.

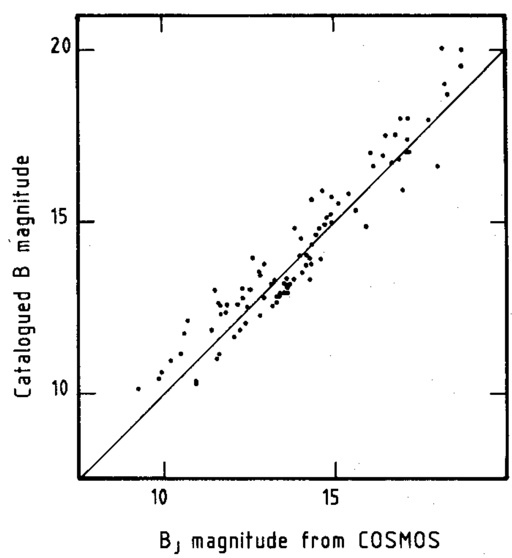

Figure 8. Plot of B-magnitude from catalogues, or in a few cases estimated off the plate, against COSMOS measured magnitude for the galaxies. The mean difference is 0.6 mag.

that the ratio of infrared to optical luminosity is given by

$$\log \frac{L(\mathrm{IR})}{L(B)} = \log(3.25F_{60}+1.26F_{100})-14-(-7.54-0.4B_J),$$

where we have put $L(B)=\nu f_\nu$ instead of $L(B)=\Delta\nu f_\nu$. This is a commonly used relationship, although $L(B)$ is then not strictly a blue luminosity, and may be a factor ~3 ($\nu/\Delta\nu$) larger than other published values (see e.g. Moorwood, Veron-Cetty & Glass 1986). The values of $L(\mathrm{IR})/L(B)$ for this sample, which consists of both cluster and background galaxies, range from 0.06 to 50, with a most populated value of 1. No internal extinction correction, which may reduce these values, has been applied. Values of $\log[L(\mathrm{IR})/L(B)]$ for these 97 galaxies are given in Table 1.

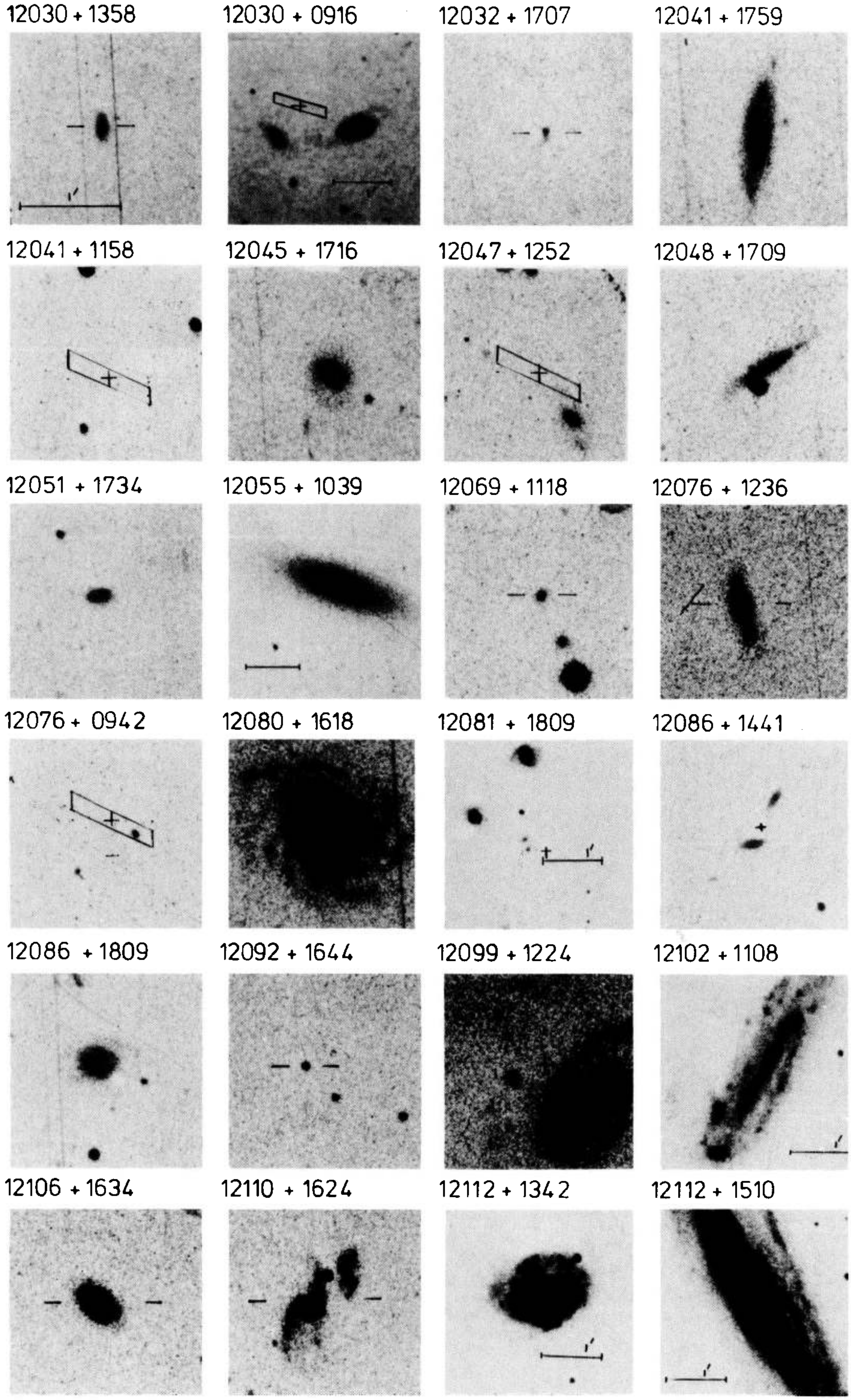

Plate 3. (a)–(g) Finding charts of the galaxies and empty fields found in this work, in RA order, 2×2 arcmin unless otherwise marked. North is at the top and east to the right.

1987MNRAS.227..563L

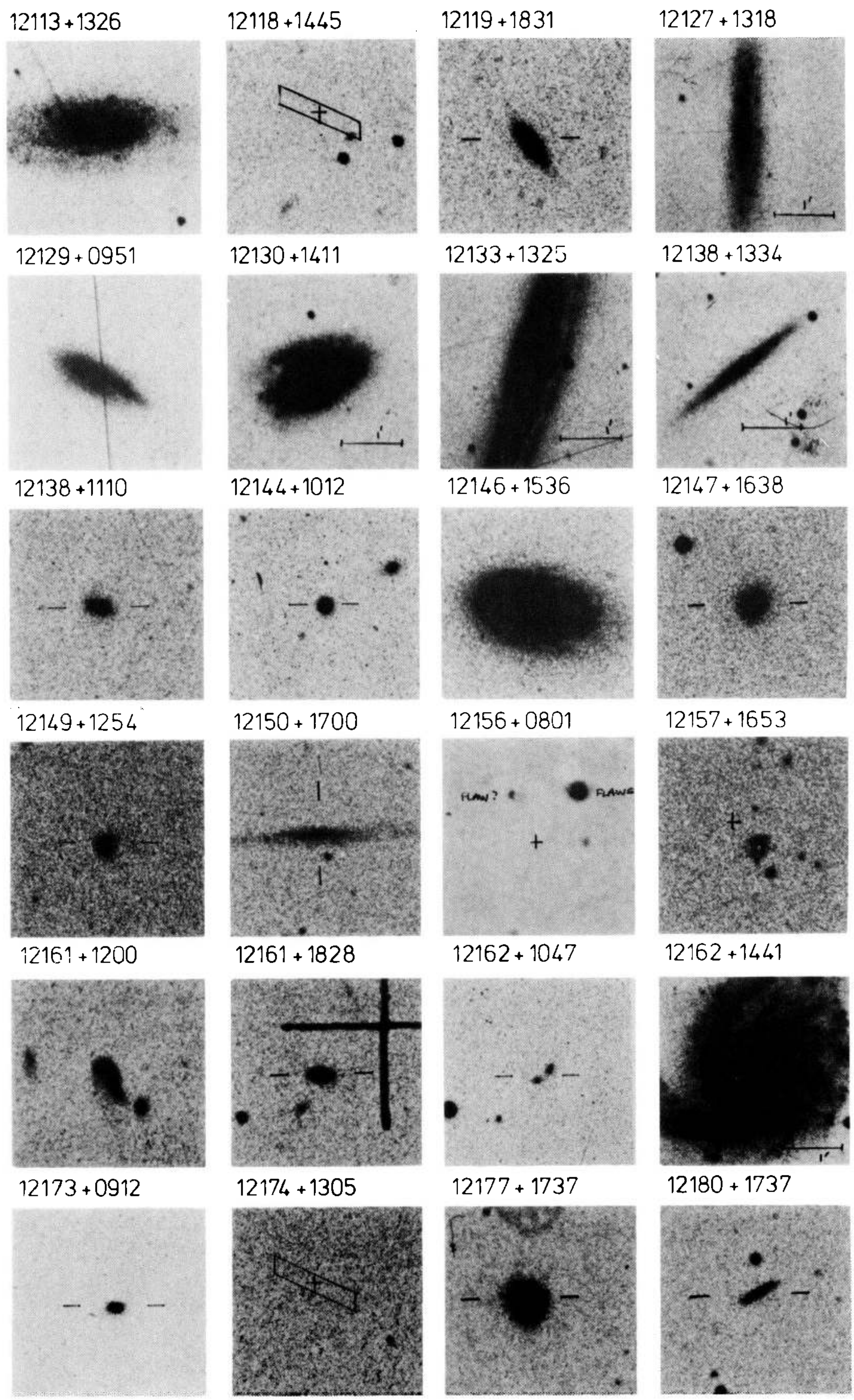

Plate 3(b)

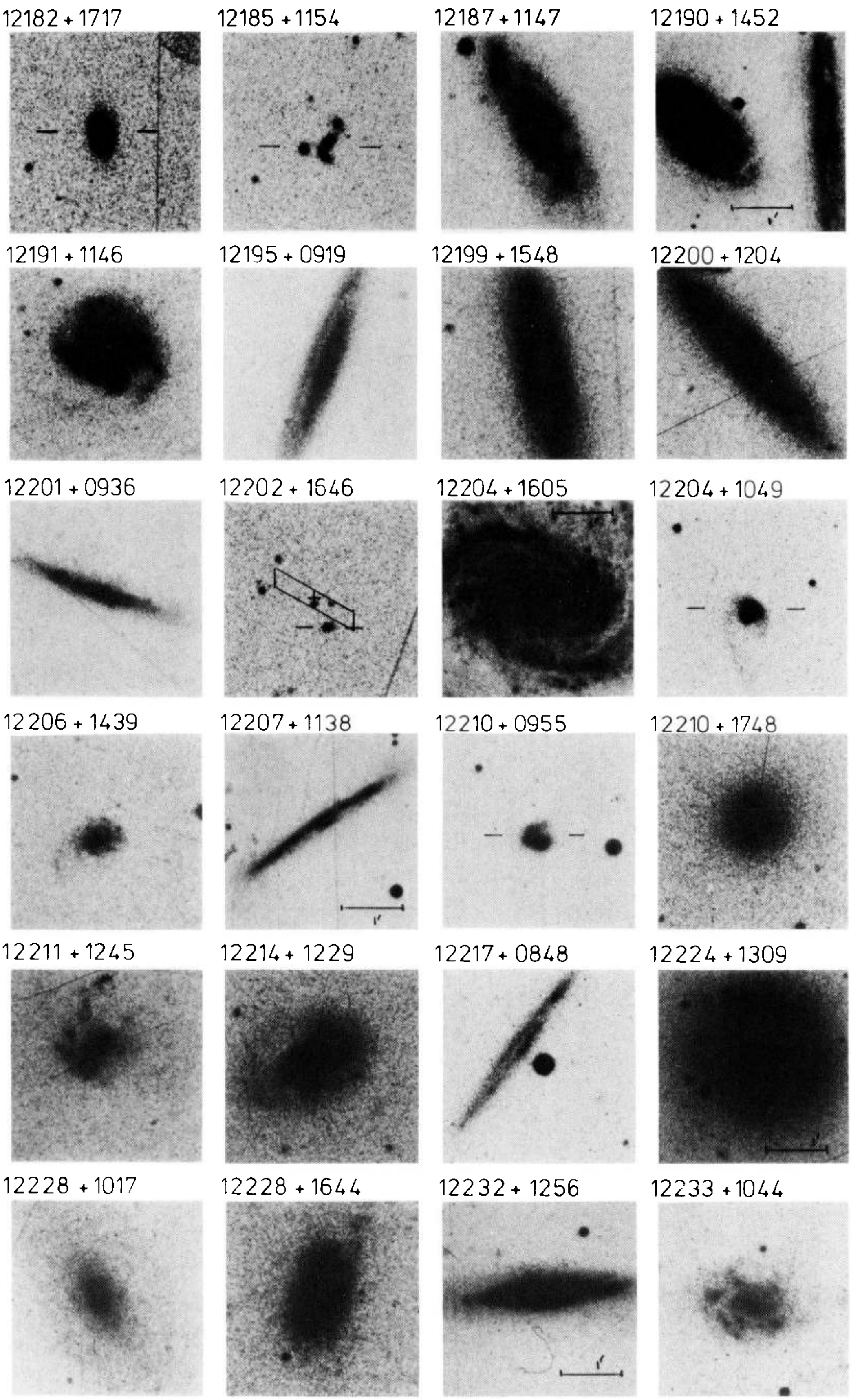
12182 + 1717
12185 + 1154
12187 + 1147
12190 + 1452
12191 + 1146
12195 + 0919
12199 + 1548
12200 + 1204
12201 + 0936
12202 + 1646
12204 + 1605
12204 + 1049
12206 + 1439
12207 + 1138
12210 + 0955
12210 + 1748
12211 + 1245
12214 + 1229
12217 + 0848
12224 + 1309
12228 + 1017
12228 + 1644
12232 + 1256
12233 + 1044

Plate 3(c)

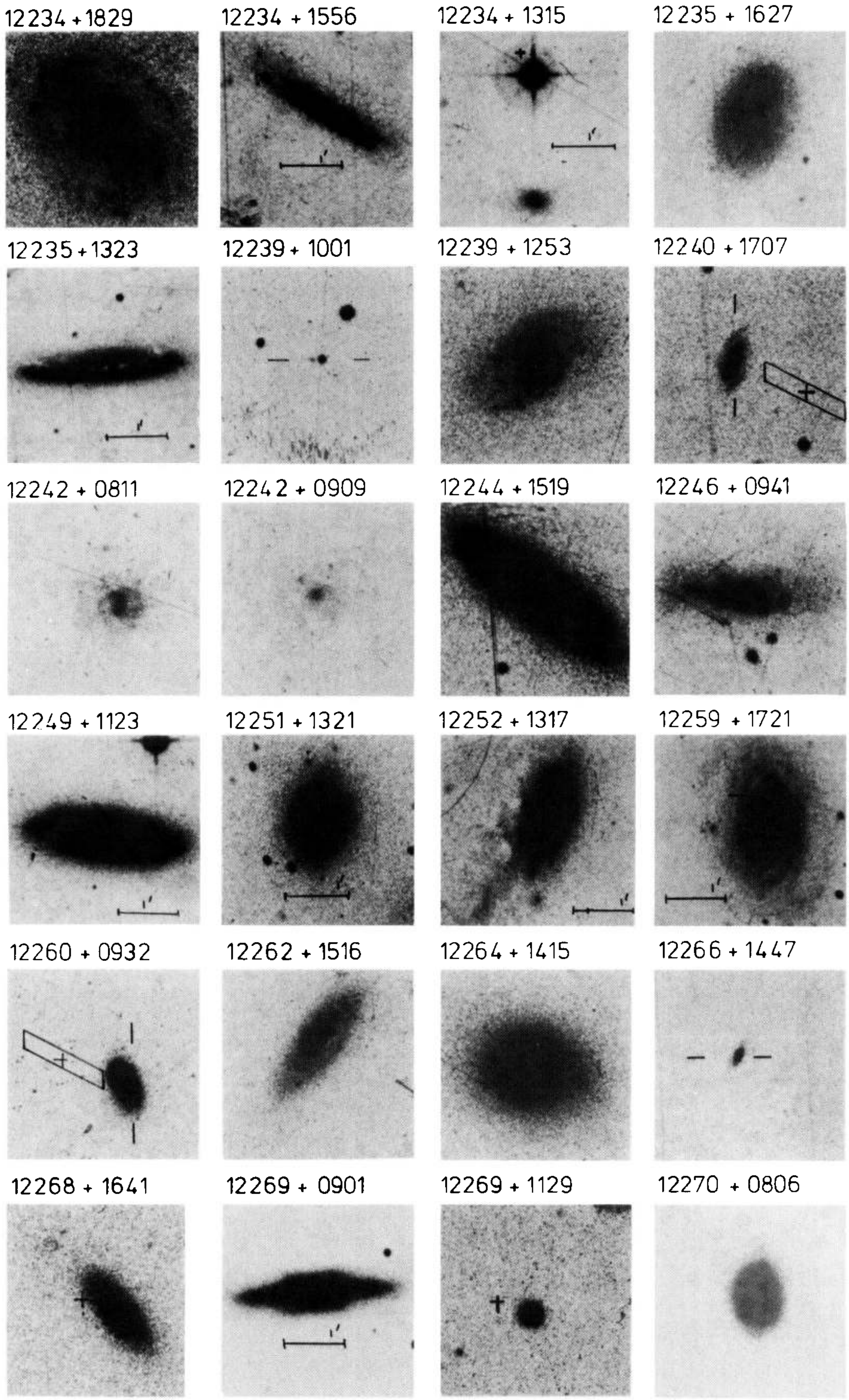
12234 + 1829
12234 + 1556
12234 + 1315
12235 + 1627
12235 + 1323
12239 + 1001
12239 + 1253
12240 + 1707
12242 + 0811
12242 + 0909
12244 + 1519
12246 + 0941
12249 + 1123
12251 + 1321
12252 + 1317
12259 + 1721
12260 + 0932
12262 + 1516
12264 + 1415
12266 + 1447
12268 + 1641
12269 + 0901
12269 + 1129
12270 + 0806

Plate 3(d)

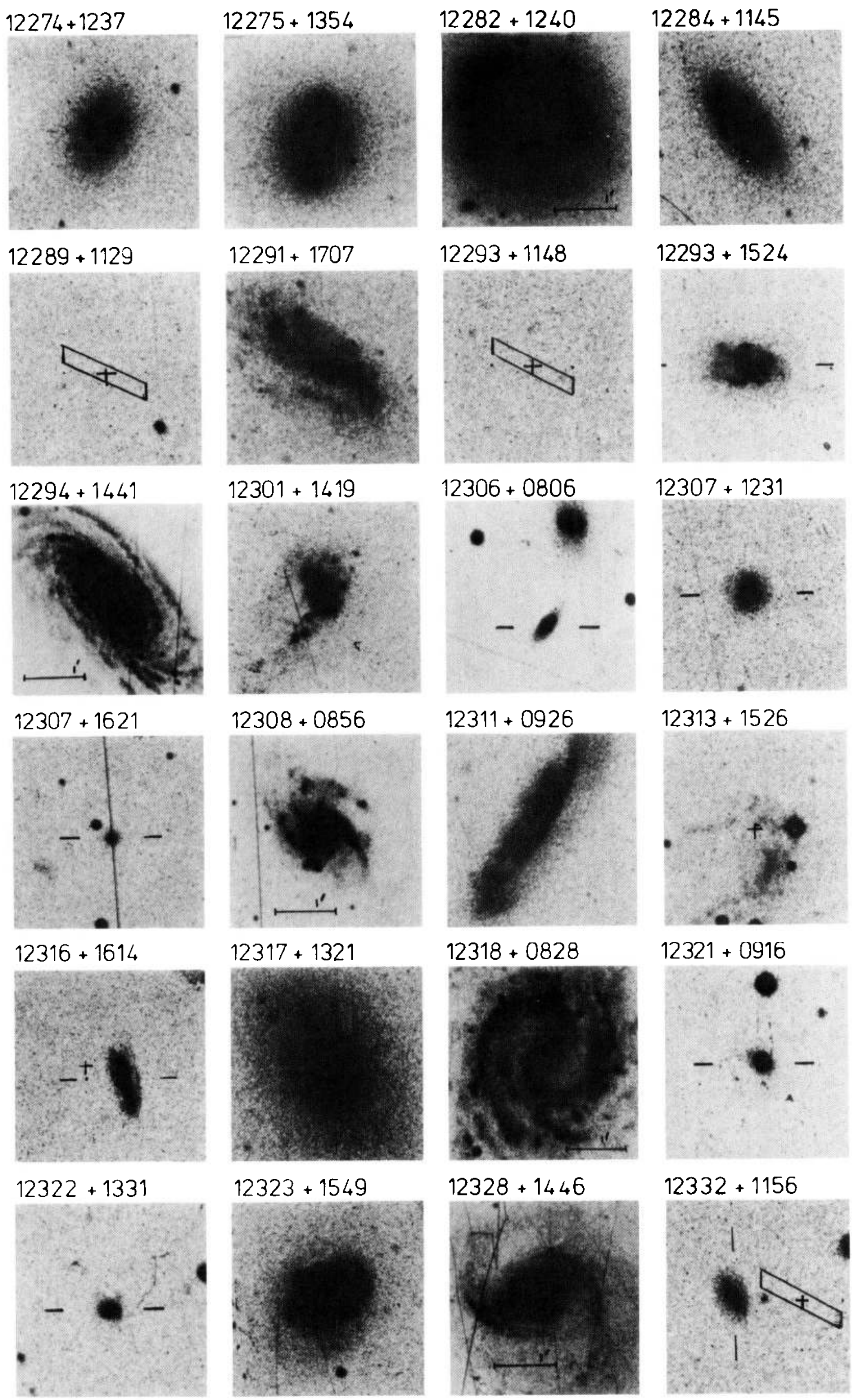
12274+1237
12275+1354
12282+1240
12284+1145
12289+1129
12291+1707
12293+1148
12293+1524
12294+1441
12301+1419
12306+0806
12307+1231
12307+1621
12308+0856
12311+0926
12313+1526
12316+1614
12317+1321
12318+0828
12321+0916
12322+1331
12323+1549
12328+1446
12332+1156

Plate 3(e)

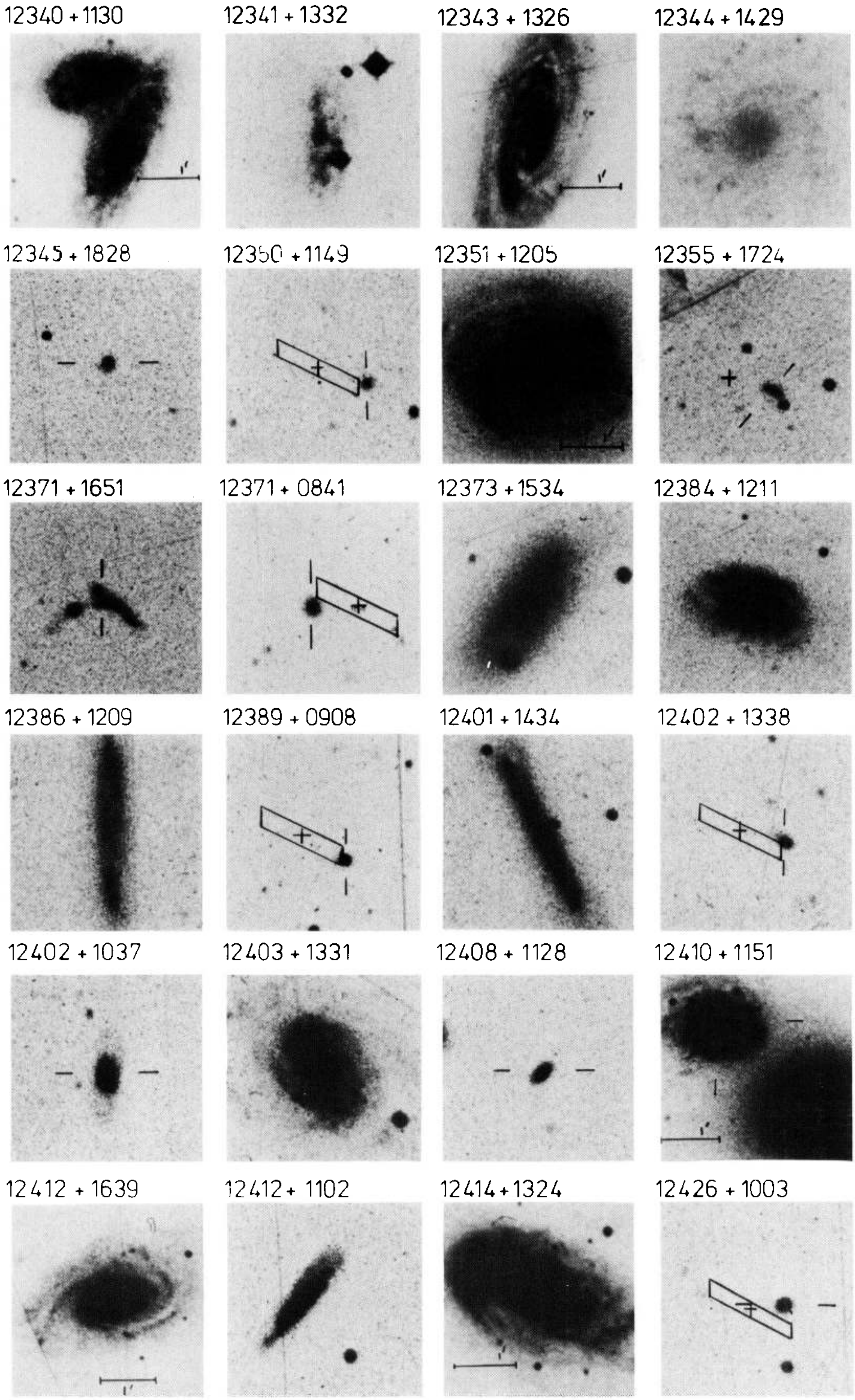
12340 + 1130
12341 + 1332
12343 + 1326
12344 + 1429
12345 + 1828
12350 + 1149
12351 + 1205
12355 + 1724
12371 + 1651
12371 + 0841
12373 + 1534
12384 + 1211
12386 + 1209
12389 + 0908
12401 + 1434
12402 + 1338
12402 + 1037
12403 + 1331
12408 + 1128
12410 + 1151
12412 + 1639
12412 + 1102
12414 + 1324
12426 + 1003

Plate 3(f)

1987MNRAS.227..563L

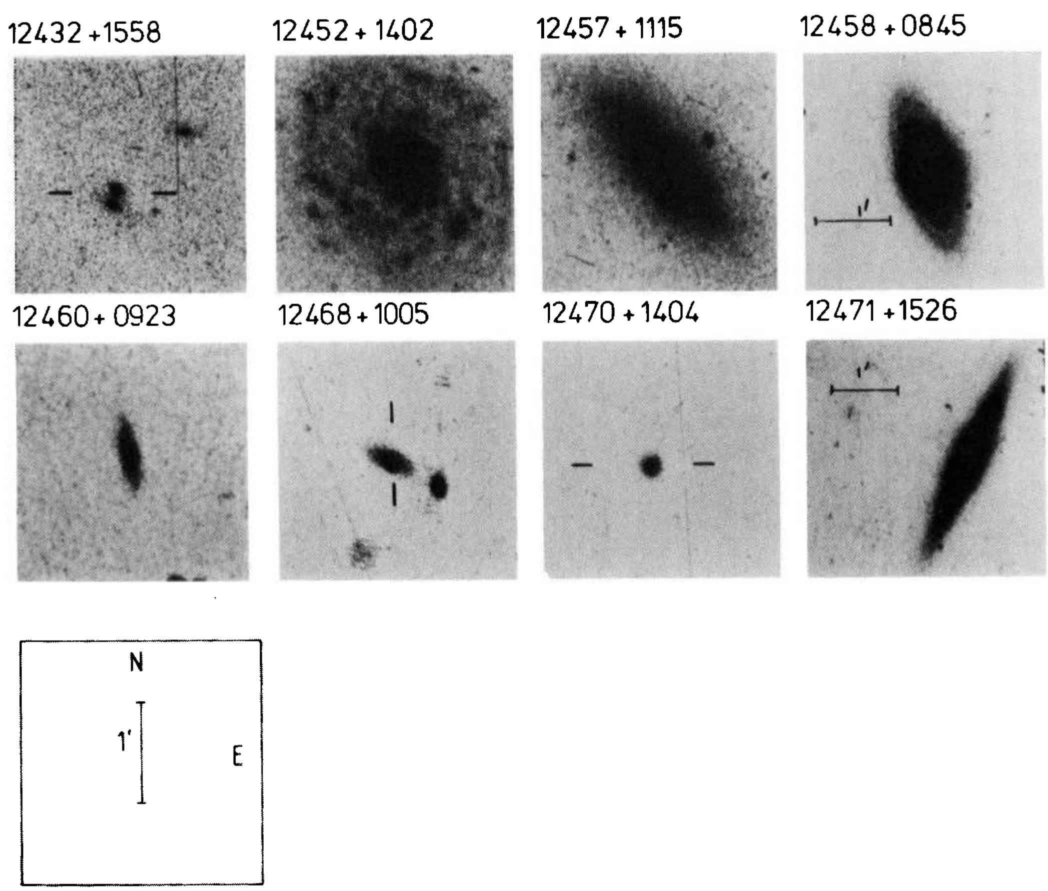

Plate 3(g)

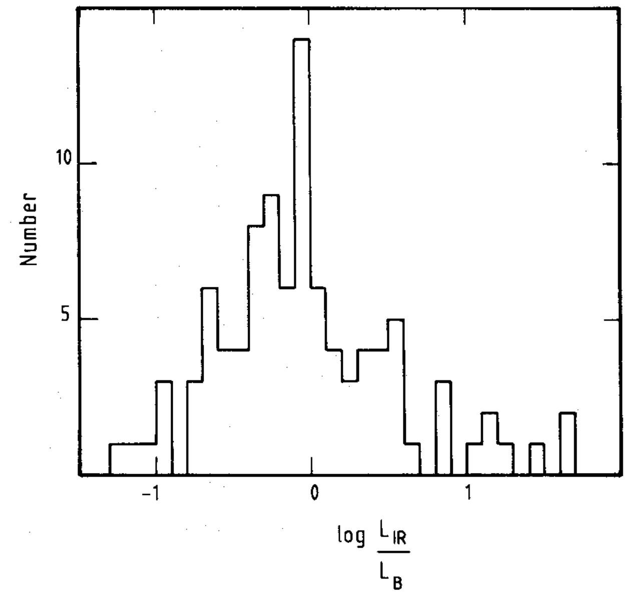

Figure 9. Distribution of the logarithm of the ratio of infrared to optical luminosity for 97 galaxies with 'cosmags' and moderate- or high-quality detections at both 60 and 100μm. $\log[L(\mathrm{IR})/L(B)]=\log[3.25F(60\mu\mathrm{m})+1.26F(100\mu\mathrm{m})]+0.4B-6.46$ (see text).

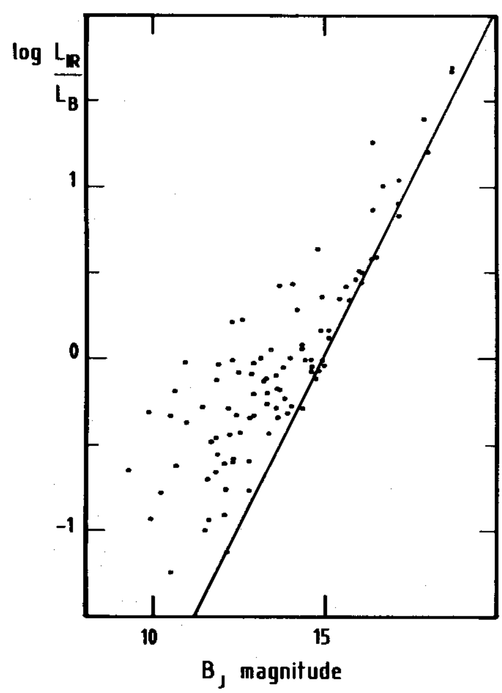

Figure 10. Plot of the logarithm of the ratio of infrared to optical luminosity for 97 galaxies with 'cosmags' and moderate- or high-quality detections at both 60 and 100μm, against 'cosmag'. The line gives the minimum value of $L(\mathrm{IR})/L(B)$, at given B, for detection by *IRAS* (see text).

In Paper 1 it was shown that for a given B, there is a minimum value of $L(\mathrm{IR})/L(B)$ for the source to be detected by *IRAS*, given by

$$\log\left[\frac{L(\mathrm{IR})}{L(B)}\right]=0.4B_J-5.95.$$

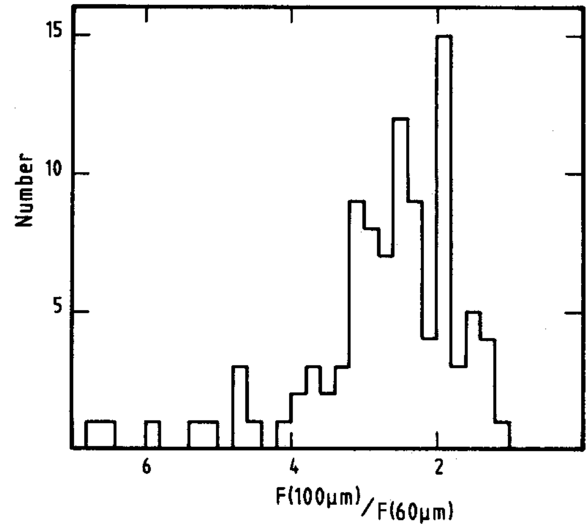

Figure 11. Distribution of the flux density ratio $F(100\mu m)/F(60\mu m)$ for 97 galaxies with 'cosmags' and moderate- or high-quality detections at both 60 and $100\mu m$.

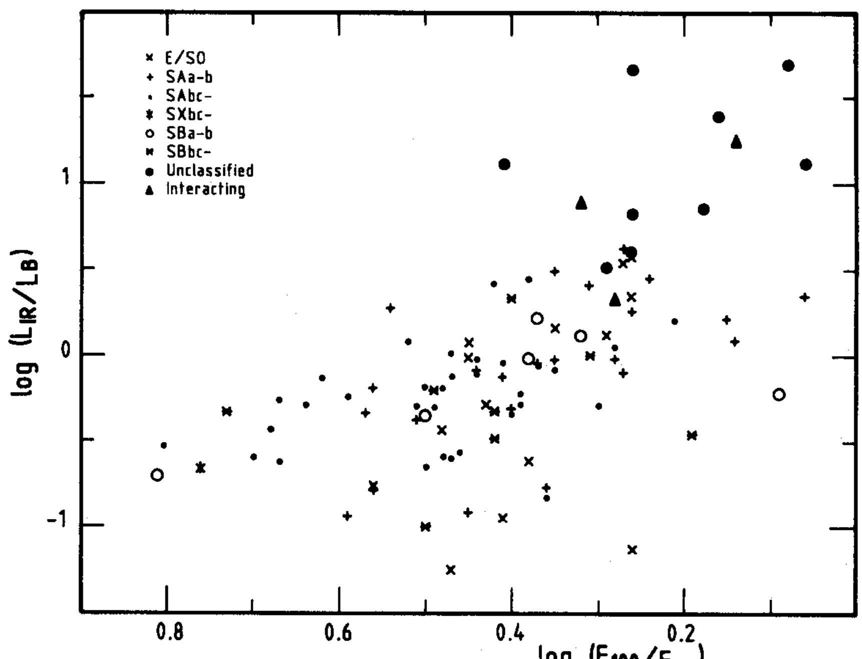

Figure 12. Plot of the logarithm of the ratio of infrared to optical luminosity against $F(100\mu m)/F(60\mu m)$ for the sample of galaxies as in Figs 10 and 11. The symbols distinguish the galaxies by type code as follows: ×, elliptical or lenticular; +, SA a–b; SX a–b (none); ○, SB a–b; ●, optically faint unclassified; ▲, interacting; ·, SA bc–; *, SX bc–; ⁎, SB bc–.

This relationship is shown in Fig. 10, which is a plot of $\log[L(\mathrm{IR})/L(B)]$ against B. It can be seen that, for a given value of B, $L(\mathrm{IR})/L(B)$ varies by about a factor of 10 in the more populated (bright) region of the diagram.

Fig. 11 shows the histogram of the ratio of the $100\mu m$ flux density to the $60\mu m$ flux density, for the same sample as Figs 9 and 10. The values range from 1 to 7, peaking at 2, with a mean value of 2.7 (which corresponds to a colour temperature of 25–50 K).

The infrared to blue luminosity and $100/60\mu m$ flux density ratio are combined in Fig. 12. The different source types are distinguished by different symbols, using the type code described at the end of Table 1. The faint unclassified galaxies and the galaxies classified as interacting have the highest value of $L(\mathrm{IR})/L(B)$, and low values of $F(100\,\mu\mathrm{m})/F(60\,\mu\mathrm{m})$. These galaxies are apparently infrared luminous and 'hot'. All spiral galaxies, barred and unbarred, have very similar values of the ratio of infrared to optical luminosity, and $F(100\,\mu\mathrm{m})/F(60\,\mu\mathrm{m})$.

The E/S0 galaxies appear to be indistinguishable from the spirals in Fig. 12. However, although there certainly are some infrared–luminous E/S0 galaxies, this result should be treated with caution as the elliptical/lenticular classification may be in error for fainter galaxies in which morphological structure is difficult to see.

The mean values of the ratios $\log[L(\mathrm{IR})/L(B)]$ and $\log[F(100\,\mu\mathrm{m})/F(60\,\mu\mathrm{m})]$ for each type are given in Table 5. The mean values of $L(\mathrm{IR})/L(B)$, $F(100\,\mu\mathrm{m})/F(60\,\mu\mathrm{m})$ are as follows: E/S0 – 1.1, 2.5; S(B) a–b – 1.5, 2.6; S(B) bc–d – 0.75, 3.2; faint – 19, 1.7; interacting – 9.5, 1.8. For the 85 spirals and elliptical/lenticulars, the mean value of $L(\mathrm{IR})/L(B)$ is $1(\pm{\sim}2)$, and of $F(100\,\mu\mathrm{m})/F(60\,\mu\mathrm{m})$ is $3(\pm{\sim}1)$.

Morphological effects on infrared properties of galaxies are discussed further in Section 5.2.

Table 5. Mean values of $\log[L(\mathrm{IR})/L(B)]$ and $\log[F(100\,\mu\mathrm{m})/F(60\,\mu\mathrm{m})]$ as a function of morphology, for the Virgo *IRAS* galaxies (present work), the SGP *IRAS* galaxies (Paper 1) and the optically selected sample of *IRAS* galaxies of de Jong *et al.* (1984).

Morphology	Mean log [L(IR)/L(B)]	Mean log [F(100μm)/F(60μm)]	No. in sample	Source
E/S0	-0.26 (0.61)	0.38 (0.10)	14	Present work
S(B)a-b	-0.07 (0.47)	0.38 (0.16)	29	
S(B)bc-d	-0.23 (0.31)	0.48 (0.14)	42	
Faint	1.10 (0.43)	0.22 (0.11)	9	
Interacting	0.84 (0.46)	0.25 (0.10)	3	
E/S0	0.62 (0.08)	0.27 (0.02)	15	Paper 1
S(B)a-b	0.30	0.35	39	
S(B)bc-d	-0.21	0.45	21	
Faint	1.24 (0.17)	0.19 (0.04)	17	
S(B)0	-0.45 (0.15)	0.32 (0.10)	6	de Jong et al.
Sa-bc	-0.37 (0.05)	0.50 (0.03)	29	
Sc-d	-0.42 (0.05)	0.52 (0.02)	29	
SBa-bc	-0.20 (0.13)	0.33 (0.04)	14	
SBc-d	-0.31 (0.10)	0.42 (0.07)	6	
Sdm,Sm,Im, Amorphous	-0.26 (0.21)	0.24 (0.10)	4	

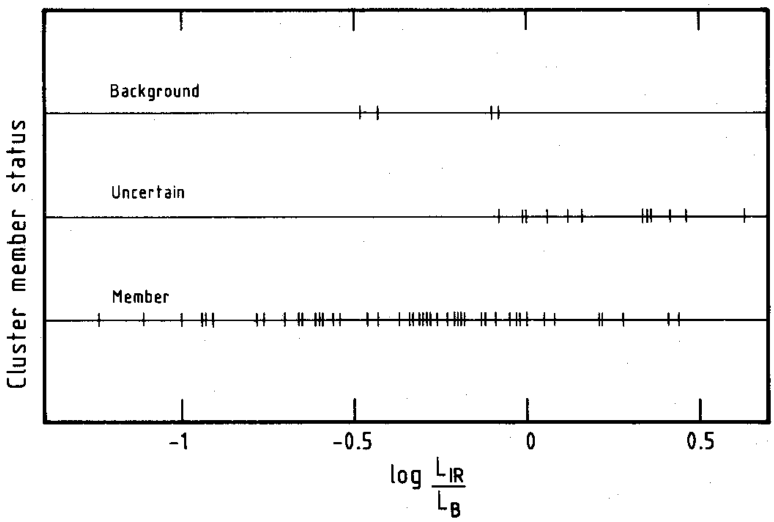

Figure 13. Plot of cluster membership status, against the logarithm of the ratio of infrared to optical luminosity, for the 75 galaxies of the sample in Figs 9, 10 and 11 that are in the Binggeli *et al.* (1985) optical Virgo cluster catalogue.

5.1.2 *The infrared–optical database*

We have paired our data with the catalogue by Binggeli *et al.* (1985). This is an optically selected sample of 2096 galaxies in an area of 140 $\deg^2$ at Virgo, which covers 77 per cent of our area (see Plate 1). Binggeli *et al.* give the likelihood of cluster membership and redshifts for many of the galaxies. Of the 97 galaxies with good 60 and 100 μm detections and 'cosmags', 75 are in their catalogue. Fig. 13 shows $\log[L(\mathrm{IR})/L(B)]$ as a function of cluster membership status. The background and uncertain cluster members have values of the ratio of infrared to blue luminosity similar to that of the cluster members with the highest values of $L(\mathrm{IR})/L(B)$.

In order to calculate luminosities for these galaxies, we have assumed that cluster members are all at the same distance of 19 Mpc, given by the mean observed heliocentric velocity (960 km s^{-1} by Binggeli *et al.*, H_0=50 km s^{-1} Mpc^{-1}); this compares with a distance of 13 Mpc derived by de Vaucouleurs (1985) from supernova observations. The uncertainty in the distance may lead to an uncertainty in the derived luminosities of about a factor of 2. There are 18 non-cluster or uncertain cluster members in the sample of 75; 16 of these have redshifts by Binggeli *et al.* and these redshifts were used to derive IR luminosities. The values of $\log[L(\mathrm{IR})]$ for the 73 galaxies are given in Table 1.

Luminosity has been plotted against the ratio of 100 and 60 μm flux density in Fig. 14, against $L(\mathrm{IR})/L(B)$ in Fig. 15, and against spiral morphology (from Binggeli *et al.* who used the Revised Shapley Ames system) in Fig. 16. Cluster, background and uncertain cluster members have been identified in these figures. The plots show that the ratio $F(100\,\mu\mathrm{m})/F(60\,\mu\mathrm{m})$ tends to decrease with increasing luminosity, and that there is a correlation between $L(\mathrm{IR})/L(B)$ and $L(\mathrm{IR})$. Although luminosities $\gtrsim 10^{10} L_\odot$ are reached only by Sb's and Sc's, luminosities of $10^9 L_\odot$ are common for the spirals in this sample.

The plot of $L(\mathrm{IR})/L(B)$ against $L(\mathrm{IR})$, Fig. 15, indicates that the majority of spiral galaxies have $0.1<L(\mathrm{IR})/L(B)<1$ and $L(\mathrm{IR})\sim 10^9 L_\odot$; these have $B\leqslant 14$ from Fig. 10. This group describes the normal, or typical, *IRAS* galaxy. Fig. 15 shows that there are also galaxies with $1<L(\mathrm{IR})/L(B)\leqslant 4$ that have a far-infrared luminosity of 10^{10}–$10^{11} L_\odot$ and, again from Fig. 10, such galaxies have $14<B\leqslant 16$. If we extrapolate the correlation between $L(\mathrm{IR})/L(B)$ and $L(\mathrm{IR})$ seen in Fig. 15 for the galaxies that are fainter than 16th magnitude at B, and that therefore have $L(\mathrm{IR})/L(B)$ between 4 and 50 (see Fig. 10), the implied $L(\mathrm{IR})$ must be between 10^{11} and $10^{13} L_\odot$.

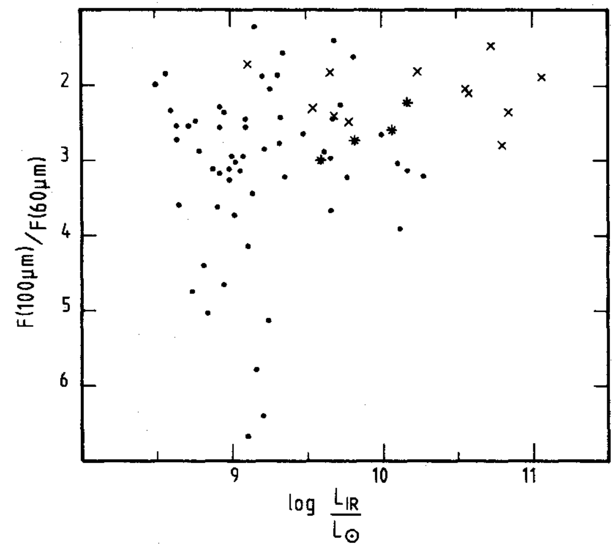

Figure 14. Plot of $F(100\mu m)/F(60\mu m)$ against luminosity for the 73 galaxies that are in the Virgo cluster (assumed distance 19 Mpc), or that have redshifts, as given by the Binggeli *et al.* (1985) optical Virgo cluster catalogue. Assumed $H_0=50\,km\,s^{-1}\,Mpc^{-1}$. Cluster membership status is distinguished as follows: ·, cluster member; ×, uncertain; *, background.

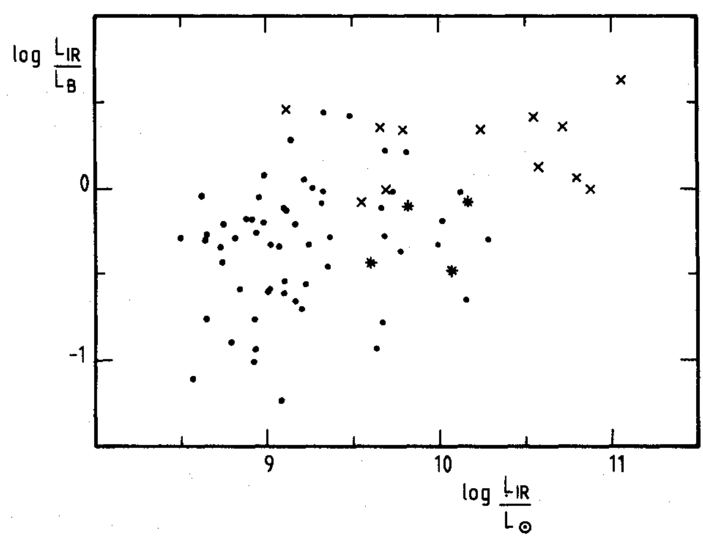

Figure 15. Plot of the logarithm of the ratio of infrared to optical luminosity against luminosity for the 73 galaxies that are in the Virgo cluster (assumed distance 19 Mpc), or that have redshifts, as given by the Binggeli *et al.* (1985) optical Virgo cluster catalogue. Assumed $H_0=50\,km\,s^{-1}\,Mpc^{-1}$. Cluster membership status is distinguished as follows: ·, cluster member; ×, uncertain; *, background.

We have obtained redshifts for some of the optically fainter galaxies identified in Paper 1 (work in progress). These measurements support the $L(IR)/L(B){:}L(IR)$ correlation, and show that galaxies with an infrared to blue luminosity ratio greater than 30 may have a far-infrared luminosity greater than $10^{12}\,L_{\odot}$, i.e. a quasar-type luminosity. About 1 in 20 of the field galaxies identified in Paper 1 have $L(IR)/L(B)>30$. This is comparable to the 1 in 30 galaxies with $L(IR)>10^{12}\,L_{\odot}$ found by Lawrence *et al.* (1986) for their samples of *IRAS* galaxies with redshifts. If the empty fields are *IRAS* galaxies with $B>22$, the implied infrared luminosity is about $10^{13}\,L_{\odot}$.

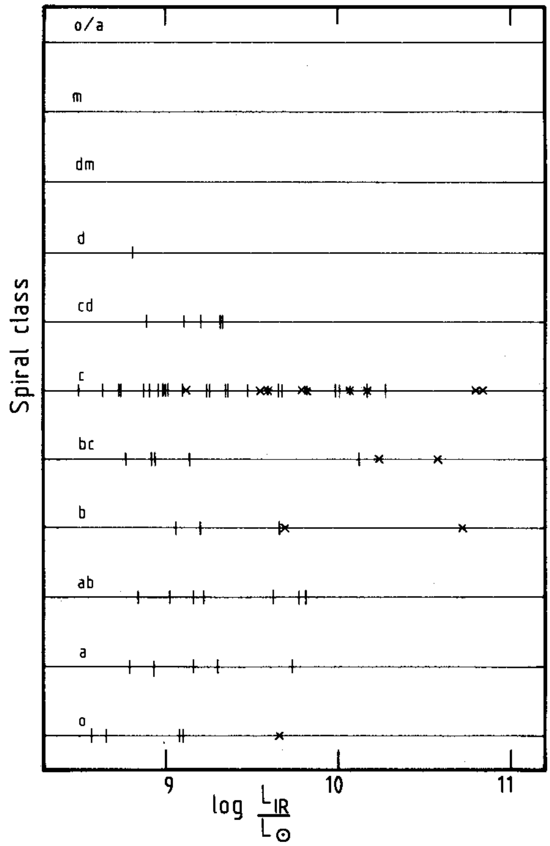

Figure 16. Plot of spiral morphology (from Binggeli *et al.* 1985) against luminosity for the 73 galaxies that are in the Virgo cluster (assumed distance 19 Mpc), or that have redshifts, as given by the Bingeli *et al.* (1985) optical Virgo cluster catalogue. Assumed $H_0=50\,\mathrm{km\,s^{-1}\,Mpc^{-1}}$. Cluster membership status is distinguished as follows: |, cluster member, ×, uncertain; *, background.

5.2 THE INFRARED PROPERTIES OF THE VIRGO CLUSTER GALAXIES COMPARED WITH FIELD GALAXIES

5.2.1 *Comparison with Paper 1, the SGP* IRAS *galaxies*

As would be expected, the present sample has a higher surface density of visually bright galaxies than the sample in Paper 1 for the SGP area. The SGP sample has an optical magnitude range of $10<B<20$, with a broad peak at 13–17, *cf.* Fig. 7. Optical studies of the Virgo cluster have indicated a low background density of galaxies (e.g. Binggeli *et al.* 1985), however, the surface density of galaxies fainter than $B=16$ detected by *IRAS* is similar for this area and the SGP area.

The *IRAS* galaxies in the SGP have higher values of $L(\mathrm{IR})/L(B)$ (0.2–158, peak values 1–3) than the Virgo galaxies. The difference is due to the different optical magnitude (or redshift) distributions of the samples. The plots of $L(\mathrm{IR})/L(B)$ against B for the two areas are very similar at the bright end, where the total number of galaxies is similar (due to the larger area covered in Paper 1). The SGP sample contains a larger number, in total, of optically faint galaxies that must have higher values of $L(\mathrm{IR})/L(B)$ for detection by *IRAS* (see Fig. 10). Because of the greater number of high $L(\mathrm{IR})/L(B)$ galaxies in the SGP sample, that sample shows a better defined relationship between $L(\mathrm{IR})/L(B)$ and $F(100\,\mu\mathrm{m})/F(60\,\mu\mathrm{m})$.

A marked difference exists between the morphological dependence of the infrared to optical luminosity ratios in the SGP and Virgo samples. It was shown in Paper 1 that early-type spirals have higher values of $L(\mathrm{IR})/L(B)$ than later types. The mean value of $\log[L(\mathrm{IR})/L(B)]$ is 0.30

for Sa–b compared with −0.21 for Sbc–d. In contrast this work shows all spirals to have log[L(IR)/L(B)] about −0.2, and although early types have a slightly higher mean value (−0.07), there is certainly no evidence of the IR-luminous early-type spirals seen in the SGP. This is discussed further below. Table 5 gives the mean values of the ratios log[L(IR)/L(B)] and log[F(100 μm)/F(60 μm)] for each galaxy type, for the Virgo and SGP samples.

5.2.2 *Comparison with other work*

Soifer *et al.* (1984) and de Jong *et al.* (1984) used the *IRAS* data to study an infrared (60 μm) selected sample of galaxies, and an optically selected sample of galaxies, respectively. Each sample consisted of about 100 galaxies. They obtained L(IR)/L(B) values of between 1 and 40 for the infrared sample, and between 0.2 and 2.5 for the optical sample. The Virgo sample of *IRAS* galaxies presented in this work is effectively an optically selected sample, as it is dominated by bright cluster galaxies, and the SGP sample is infrared selected (field galaxies detected by *IRAS*). Therefore it is not surprising that the Virgo galaxies have similar values of L(IR)/L(B) to the optically selected sample of de Jong *et al.* or that the SGP sample is very similar to the IR sample of Soifer *et al.*

Moorwood *et al.* (1986) have made optical and near-infrared observations of 22 of the *IRAS* galaxies in the infrared selected sample of Soifer *et al.* They have compared these galaxies with a sample of 100 normal disc galaxies chosen by Kennicutt (1983) for a study of star formation rates. They find that up to 50 per cent of the Soifer *et al.* sample suffer abnormally high internal absorption, which may account for the higher L(IR)/L(B) ratios compared with optically selected samples. However, there is evidence that the Soifer *et al.* mini-survey unfortunately contains galaxies with unusually high internal extinction, as Soifer *et al.* do not find any correlation between L(IR)/L(B) and F(100 μm)/F(60 μm); other samples of *IRAS* galaxies do show this correlation. The correlation is seen in both optical and infrared selected samples (e.g. those of de Jong *et al.* and Paper 1).

Moorwood *et al.* find that the far-infrared luminosity correlates well with integrated H alpha luminosity. As this is proportional to the current star formation rate (SFR), and the blue luminosity is proportional to the average SFR, L(IR)/L(B) is a measure of the ratio of current to average SFR, and, after dereddening, Moorwood *et al.* found these values to be consistent with normal rates of disc star formation. They conclude that a spiral disc which had evolved uniformly with time would have a value of L(IR)/L(B) around 0.5 [with our L(B) definition], with a scatter of about a factor of 3 being normal. This is very similar to the Virgo cluster galaxies, implying that the star formation rate in cluster and non-cluster galaxies is similar.

Young *et al.* (1984) studied *IRAS* sources in the Hercules cluster. They find a notable lack of E and S0 galaxies, and derive luminosities between 10^9 and $10^{10} L_\odot$ as we find in this study of the Virgo cluster. It appears that these cluster environments do not affect the infrared properties of galaxies. Furthermore, these properties have been unaffected by the stripping of neutral hydrogen that has occurred in the inner regions of the Virgo cluster.

The far-infrared properties of the Virgo cluster galaxies and field galaxies in fact appear to be indistinguishable. Rieke & Lebofsky (1986) have used the *IRAS* data to make a careful study of the infrared properties of an unbiased, volume-limited sample of about 300 field galaxies. The present work, dominated by the cluster galaxies, agrees with their findings, reproducing the values and relationships between L(IR) and F(100 μm)/F(60 μm), L(IR) and L(IR)/L(B), as well as L(IR) and morphology. That is, they also find that L(IR) correlates with F(100 μm)/F(60 μm) and L(IR)/L(B), and that Sb–c spirals are the most luminous galaxy type, reaching luminosities of $10^{10} L_\odot$.

Further comparisons between Virgo cluster galaxies and redshift-limited samples of field galaxies have been made by Devereux, Becklin & Scoville (1987). They compared mid-infrared fluxes and *IRAS* fluxes for a sample of 50 Virgo cluster galaxies and a sample of 36 field galaxies at a similar redshift, and find no difference in either 10 μm or FIR (60+100 μm) luminosity between the two samples. Devereux *et al.* also find that there is no dependence of nuclear IR luminosity on morphology, but the discs of Sc galaxies are typically 3–4 times more luminous than Sa discs. They conclude that the global star formation rate in late-type spirals is typically twice that of the early-type spirals. The present work agrees with these findings, however in contrast our SGP sample showed early-type spirals (Sa–b) to be the most infrared luminous.

It appears that the central regions of spiral galaxies may become important at high luminosities, such that bars and early spiral types show an increased luminosity over disc-dominated later types. Hawarden *et al.* (1986) and de Jong *et al.* find evidence for increased IR luminosity in barred spiral galaxies. Hawarden *et al.* (Puxley, private communication) and also Devereux (1987) show that early-type barred galaxies (Sb and earlier) have enhanced luminosity in their central regions. All the samples that show this enhanced luminosity are more IR-luminous than the Virgo sample.

Table 5 summarizes the mean values of $\log[L(\mathrm{IR})/L(B)]$ and $\log[F(100\,\mu\mathrm{m})/F(60\,\mu\mathrm{m})]$, as a function of morphological type, for various samples. The definition of far-infrared luminosity used by de Jong *et al.* is slightly different from that of the other samples, but the effect should be <10 per cent, or ~0.03 in the log.

5.3 *IRAS* AND NON-*IRAS* GALAXIES

A comparison of the density of Virgo galaxies in the optical sample of Binggeli *et al.* (1985) – 15 per square degree down to B~17 – with the density of the *IRAS* galaxies studied here – 1.3 per square degree – immediately demonstrates that *IRAS* detected only a small fraction of the Virgo galaxies.

To compare the optical and infrared Virgo galaxies we have defined the following samples. First, the right ascension and declination range of our *IRAS* sample and the Binggeli sample were restricted, to ensure complete overlap, to $12^{\mathrm{h}}\,10^{\mathrm{m}}<\mathrm{RA}<12^{\mathrm{h}}\,40^{\mathrm{m}}$, $9°<\mathrm{Dec}<16°$. Stars and empty fields were excluded from the *IRAS* sample. It was found that each *IRAS* galaxy was picked up as a single member of the optical sample only if the magnitude range was restricted to $B\leqslant16$ (fainter galaxies were not always in the Binggeli *et al.* catalogue), and the position mismatch was restricted to $B\leqslant60$ arcsec (a greater tolerance led to more than one galaxy being associated with the *IRAS* galaxy). Binggeli *et al.* state that their catalogue is complete to $B\sim18$, and the restriction to $B\leqslant16$ is necessary presumably because of errors in their and our magnitudes. This procedure resulted in 65 galaxies in the detected sample, leaving 324 in the undetected sample.

Fig. 17 shows a histogram of the *B*-magnitudes (from Binggeli *et al.*) for the detected and undetected galaxies. Apart from the one galaxy with $B=9$, there is no magnitude at which *IRAS* detected all galaxies. Fig. 18 examines the populations by basic morphological type. There are a large number of elliptical galaxies of which two (for the sample defined as above) are detected by *IRAS*. The spiral-type distribution, in Fig. 19, shows that Sa–d type galaxies are frequently detected; for example 44 per cent of Sc's brighter than $B=16$ are detected.

Plotting spiral-type class against *B*-magnitude for both galaxy sets, Fig. 20, shows that *IRAS* detects nearly all spirals of type ab and later which are brighter than 14th magnitude at *B*. Eighty-eight per cent of Sc's brighter than $B=14$ are detected. It is interesting that a 14th magnitude galaxy must have $L(\mathrm{IR})/L(B)\geqslant0.4$ to be detected at both 60 and 100 μm, and this does constitute the normal *IRAS* galaxy as discussed in Section 5.1.2. The typical *IRAS* galaxy, as previously

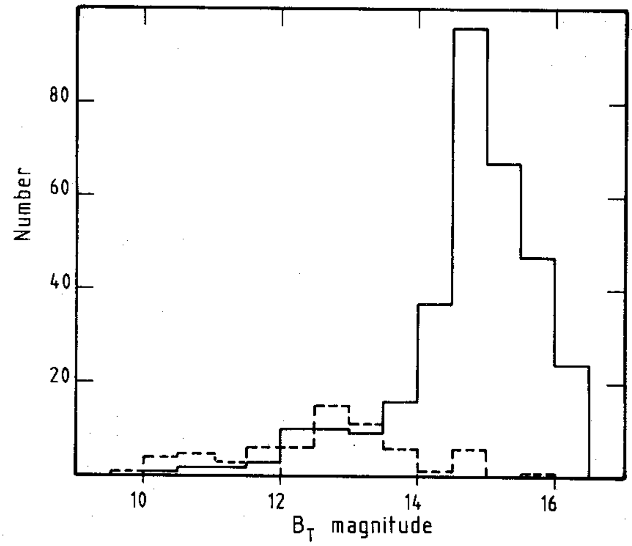

Figure 17. Distribution of *B*-magnitudes (from Binggeli *et al.* 1985) for galaxies detected by *IRAS* (65), dashed line, and undetected by *IRAS* (324), solid line, for all galaxies with $B \leq 16$, and in the region $12^h 10^m < RA < 12^h 40^m$, $9° < Dec < 16°$.

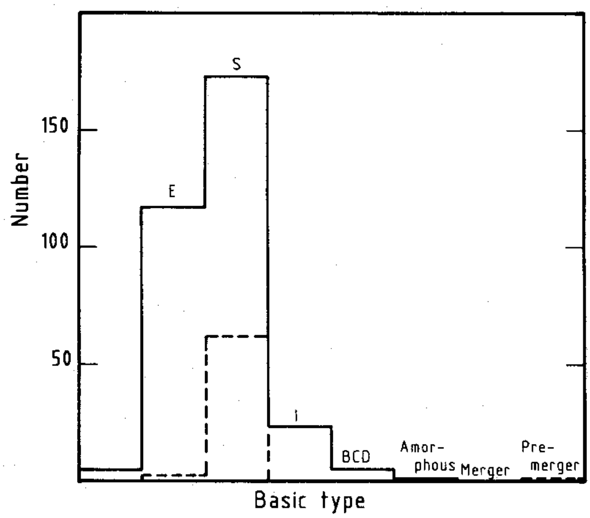

Figure 18. Distribution of basic type (from Binggeli *et al.* 1985) for galaxies detected by *IRAS* (65), dashed line, and undetected by *IRAS* (324), solid line, for all galaxies with $B \leq 16$, and in the region $12^h 10^m < RA < 12^h 40^m$, $9° < Dec < 16°$. The first, unlabelled, bin represents classified galaxies.

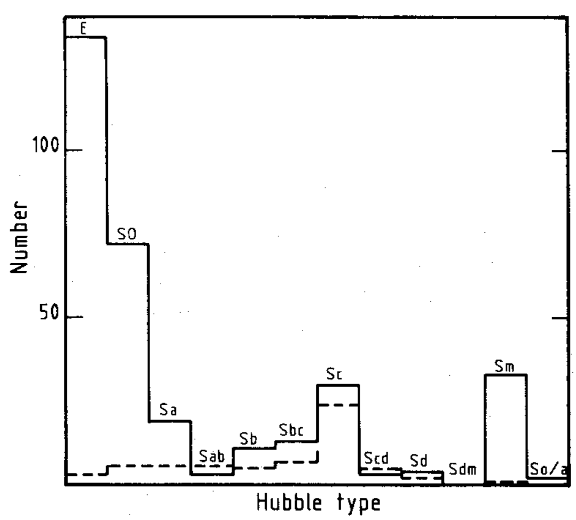

Figure 19. Distribution of spiral type (from Binggeli *et al.* 1985) for galaxies detected by *IRAS* (65), dashed line, and undetected by *IRAS* (324), solid line, for all galaxies with $B \leq 16$, and in the region $12^h 10^m < RA < 12^h 40^m$, $9° < Dec < 16°$.

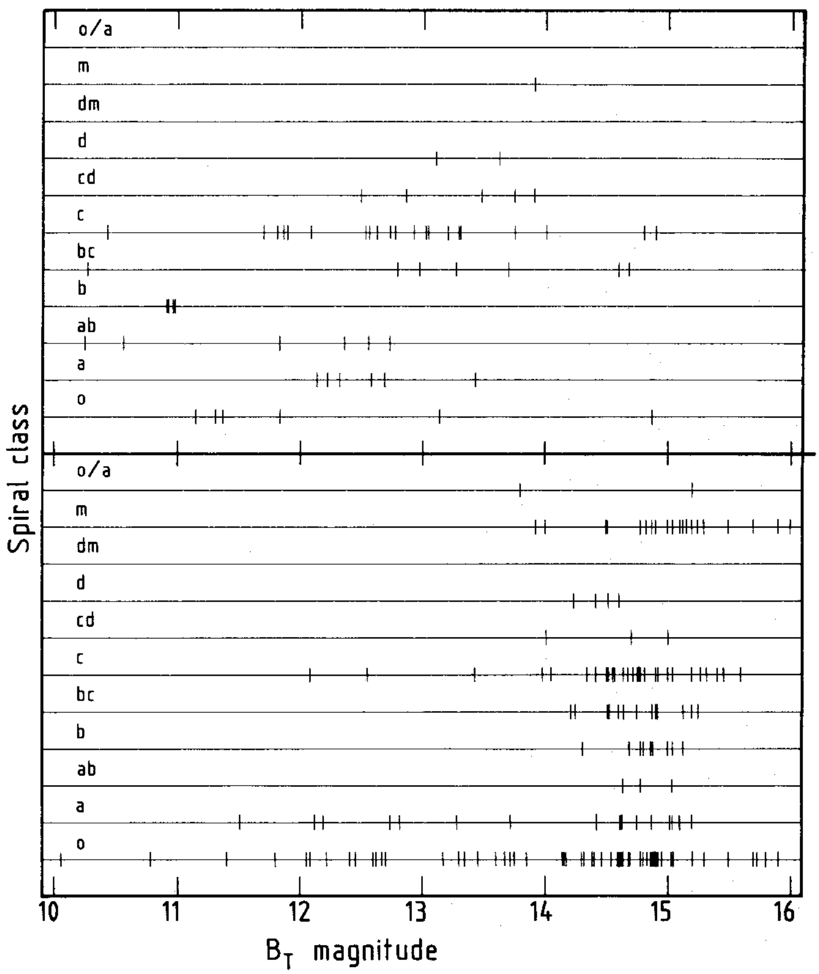

Figure 20. Plot of spiral type class (from Binggeli *et al.* 1985) against *B*-magnitude, for galaxies detected by *IRAS* (65), shown in the upper plot, and undetected by *IRAS* (324), shown in the lower plot, for all galaxies with $B \leqslant 16$, and in the region $12^h 10^m < RA < 12^h 40^m$, $9° < Dec < 16°$.

described, is a spiral galaxy (class a–d) with $B \leqslant 14$, $L(IR)/L(B)$ between 0.1 and 1, and $L(IR) \sim 10^9 L_\odot$.

6 Conclusions

6.1 THE IDENTIFICATIONS

We have found that 97 per cent of *IRAS* sources are optically identifiable above the UK Schmidt plate limit of $B=22$, both in this work and in Paper 1. This paper has given identifications for 199 of the 206 point sources detected by *IRAS* in a 113 deg^2 area centred on the Virgo cluster. Fifty-four of the sources are associated with stars, 145 with galaxies, and of the seven apparently empty fields five are very probably due to cirrus. Two sources, both detected at 60 μm only, are possibly true empty fields. The stellar sources are dominated by K-type stars, and all such stars brighter than $V=8$ are detected by *IRAS*.

6.2 THE INFRARED–OPTICAL VIRGO GALAXY DATABASE

This work presents an infrared–optical Virgo galaxy database, complete to about $B=16$, created by combining the *IRAS*–COSMOS data with the optical catalogue by Binggeli *et al.* (1985). This has allowed us to study various aspects of the Virgo galaxies, both detected and not detected by *IRAS* and compare our findings with a large amount of published data on the infrared properties of the Virgo cluster and field galaxies. Our findings on the whole have confirmed previous conclusions, but we have been able to pull together many studies and put the following conclusions on a firm quantitative basis.

Our main conclusions are

(i) The *IRAS* galaxy sources are dominated by spirals; for galaxies with $B \leq 16$ only 4 per cent of the ellipticals and lenticulars are detected, compared with 44 per cent of the Sc galaxies. Eighty-eight of Sc's brighter than $B=14$ are detected.

(ii) The cluster galaxies define a 'normal' *IRAS* galaxy. That is, the majority of *IRAS* galaxies have the same properties as a Virgo cluster *IRAS* galaxy. Such a galaxy is a spiral of type Sa–d, with $B<14$, a ratio of infrared to optical luminosity about 1, $F(100\,\mu m)/F(60\,\mu m)$ about 3, and an infrared luminosity of $\sim 10^9\,L_\odot$. For a given B, $L(\mathrm{IR})/L(B)$ can vary by a factor of about 10. These properties show the Virgo spirals to be indistinguishable from field disc galaxies with normal star formation rates.

(iii) The infrared properties of the Virgo cluster galaxies are the same as those of field galaxies at similar redshifts. Thus this cluster environment has no effect on IR properties. This is true even of the very H I deficient galaxies.

(iii) Far-infrared luminosity is correlated with $F(100\,\mu m)/F(60\,\mu m)$ and $L(\mathrm{IR})/L(B)$. The optically faint background galaxies and the interacting galaxies are 'hotter' and more infrared luminous. Galaxies with $B>16$, $L(\mathrm{IR})/L(B)>4$, and $F(100\,\mu m)/F(60\,\mu m)<2$ may have $L(\mathrm{IR})>10^{11}\,L_\odot$. Redshifts obtained for faint field *IRAS* galaxies show that galaxies with $L(\mathrm{IR})/L(B)>30$ may be ultraluminous with $L(\mathrm{IR}) \gtrsim 10^{12}\,L_\odot$; this applies to about 1 in 20 field *IRAS* galaxies. If empty fields are *IRAS* galaxies with $B>22$, this implies $L(\mathrm{IR}) \sim 10^{13}\,L_\odot$.

(v) There is some evidence that at higher infrared luminosities than that of Virgo cluster galaxies, the central regions of spiral galaxies become more important. This leads to Sb and earlier spiral types, and barred galaxies, showing higher values of $L(\mathrm{IR})/L(B)$ in more infrared luminous samples. The SGP (Paper 1) is such a sample.

The *IRAS*–COSMOS identification database can be supplied on tape if required. Please send a 600 ft tape and state if the tape is to be read on a VAX or non-VAX machine.

Acknowledgments

SKL acknowledges a SERC Research Fellowship, and a PJP a SERC Studentship. We are grateful to B. Binggeli for supplying the tape version of the Binggeli *et al.* Virgo cluster catalogue; to STARLINK and the *IRAS* Post Mission Analysis Facility at the Rutherford Appleton Laboratory for *IRAS* software, and to J. Barrow and C. Davenhall for help with its local implementation. We also thank M. Fretwell for the diagrams, and the UK Schmidt Telescope Unit and the Image Data Processing Unit at ROE for providing the plates and the COSMOS data, respectively.

References

Allen, C. W., 1973. *Astrophysical Quantities*, 3rd edn, Athlone Press, London.
Beichman, C. A., Neugebauer, G., Habing, H. J., Clegg, P. E. & Chester, T. J. (eds), 1985. *Explanatory Supplement to the IRAS Catalogues and Atlases*, US Government Printing Office, Washington DC.
Binggeli, B., Sandage, A. & Tammann, G. A., 1985. *Astr. J.*, **90**, 1681.
de Jong, T., Clegg, P. E., Soifer, B. T., Rowan-Robinson, M., Habing, H. J., Houck, J. R., Aumann, H. H. & Raimond, E., 1984. *Astrophys. J.*, **278**, L67.
de Vaucouleurs, G., 1959. *Handbook of Physics, Astrophysics IV: Stellar Systems 8*, p. 275.

de Vaucouleurs, G., 1985. *ESO Workshop on the Virgo Cluster of Galaxies,* eds Richter, O.-G. & Binggeli, B., European Southern Observatory, Garching.

Devereux, N. A., 1987. *Proc. 2nd IRAS Conference, Star Formation in Galaxies,* in press.

Devereux, N. A., Becklin, E. E. & Scoville, N., 1987. *Astrophys J.,* **312,** 529.

Hawarden, T. G., Mountain, C. M., Leggett, S. K. & Puxley, P. J., 1986. *Mon. Not. R. astr. Soc.,* **221,** 41P.

Hoffleit, D., 1982. *Bright Star Catalogue.* Yale University Observatory.

Kennicutt, R. C., 1983. *Astrophys. J.,* **272,** 54.

Lawrence, A., Walker, D., Rowan-Robinson, M., Leech, K. J. & Penston, M. V., 1986. *Mon. Not. R. astr. Soc.,* **219,** 687.

Lonsdale, C. J., Helou, G., Good, J. C. & Rice, W., 1985. *Cataloged Galaxies and Quasars Observed in the IRAS Survey,* JPL.

MacGillivray, H. T. & Stobie, R. S., 1984. *Vistas Astr.,* **27,** 433.

Moorwood, A. F. M., Veron-Cetty, M.-P. & Glass, I. S., 1986. *Astr. Astrophys.,* **160,** 39.

Olnon, F. M., Baud, B., Habing, H. J., de Jong, T., Harris, S. & Pottasch, S. R., 1984. *Astrophys. J.,* **278,** L41.

Rieke, G. H. & Lebofsky, M. J., 1986. *Astrophys. J.,* **304,** 326.

Sandage, A., Binggeli, B. & Tammann, G. A., 1985. *Astr. J.,* **90,** 1759.

Soifer, B. T. *et al.,* 1984. *Astrophys. J.,* **278,** L71.

Waters, L. B. F. M., Cote, J. & Aumann, H. H., 1987. *Astr. Astrophys.,* **172,** 225.

Wolstencroft, R. D., Savage, A., Clowes, R. G., MacGillivray, H. T., Leggett, S. K. & Kalafi, M., 1986. *Mon. Not. R. astr. Soc.,* **223,** 279 (Paper I).

Young, E., Soifer, B. T., Low, F. J., Neugebauer, G., Rowan-Robinson, M., Milney, G., Clegg, P. E., de Jong, T. & Gautier, T. N., 1984. *Astrophys. J.,* **278,** L75.